Available online at www.sciencedirect.com
ScienceDirect
Journal of the European Ceramic Society 29 (2009) 995–1011
www.elsevier.com/locate/jeurceramsoc

Review

Densification of ZrB_2-based composites and their mechanical and physical properties: A review

Shu-Qi Guo *

Composites and Coatings Center, National Institute for Materials Science, 1-2-1 Sengen, Tsukuba, Ibaraki 305-0047, Japan

Received 21 August 2008; received in revised form 27 October 2008; accepted 4 November 2008
Available online 20 December 2008

Abstract

This study reviews densification behaviour, mechanical properties, thermal, and electrical conductivities of the ZrB_2 ceramics and ZrB_2-based composites. Hot-pressing is the most commonly used densification method for the ZrB_2-based ceramics in historic studies. Recently, pressureless sintering, reactive hot pressing, and spark plasma sintering are being developed. Compositions with added carbides and disilicides displayed significant improvement of densification and made pressureless sintering possible at $\leq$2000 °C. Reactive hot-pressing allows *in situ* synthesizing and densifying of ZrB_2-based composites. Spark plasma sintering displays a potential and attractive way to densify the ZrB_2 ceramics and ZrB_2-based composites without any additive. Young's modulus can be described by a mixture rule and it decreased with porosity. Fracture toughness displayed in the ZrB_2-based composites is in the range of 2–6 MPa $m^{1/2}$. Fine-grained ZrB_2 ceramics had strengths of a few hundred MPa, which increased with the additions of SiC and $MoSi_2$. The small second phase size and uniform distribution led to higher strengths. The addition of nano-sized SiC particles imparts a better oxidation resistance and improves the strength of post-oxidized ZrB_2-based ceramics. In addition, the ZrB_2-based composites showed high thermal and electrical conductivities, which decreased with temperature. These conductivities are sensitive to composition, microstructure and intergranular phase. The unique combinations of mechanical and physical properties make the ZrB_2-based composites attractive candidates for high-temperature thermomechanical structural applications.

Keywords: Zirconium diborides; Densification; Mechanical properties; Thermal and electrical conductivities

Contents

* Tel.: +81 29 859 2223; fax: +81 29 859 2401.
E-mail address: GUO.Shuqi@nims.go.jp.

0955-2219/$ – see front matter © 2008 Elsevier Ltd. All rights reserved.
doi:10.1016/j.jeurceramsoc.2008.11.008

1. Introduction

Structural materials for use in high-temperature oxidizing environments are presently limited to SiC, Si_3N_4, oxide ceramics, and composites of these materials. Silicon-based ceramics are oxidation resistant up to ~1600 °C, due to the formation of a protective SiO_2 surface film.[1,2] Although SiO_2 is an excellent oxidation barrier at temperatures below 1600 °C, and above this temperature it begins to soften dramatically and develops substantial vapour pressure.[1,2] Therefore, the use temperature of the silicon-based ceramics is limited to 1600 °C by their thermal stability in an oxidizing atmosphere. In addition, there are a relatively few refractory oxides that are stable in an oxidizing environment at or above 2000 °C. Among these oxides, zirconia (ZrO_2) and hafnia (HfO_2) typically have the highest melting points, ~2700 °C and ~2800 °C,[1,3] respectively. Although they are inert chemically, they appear to remain susceptible to thermal shock, and exhibit high creep rates and phase transition at higher temperatures.[1,3,4] Therefore, the development of structural materials for use in oxidizing environments at temperatures above 1600 °C is of great engineering importance.

Ceramics based on the transition metal borides, nitrides, and carbides have extremely high melting points (>2500 °C) and are referred to as ultra-high temperature ceramics.[1,5] Within the family of transition metal ultra-high temperature ceramics, diborides such as ZrB_2 and HfB_2 have unique combinations of mechanical and physical properties, including high melting points (>3000 °C), high thermal and electrical conductivities, chemical inertness against molten metals, and great thermal shock resistance.[1,5,6] Thus, although carbides typically have the highest melting points (>3500 °C), the diborides ZrB_2 and HfB_2 are more attractive candidates for high-temperature thermomechanical structural applications at a temperature ≥2000 °C.[1,5] Potential applications for the diborides include thermal protective structures for leading-edge parts on hypersonic re-entry space vehicles,[1,7] propulsion systems,[1,7] furnace elements,[8] refractory crucibles,[8] and plasma-arc electrodes.[8,9] In particular, ZrB_2 has the lowest theoretical density among the ultra-high temperature ceramics, which makes it an attractive material for aerospace applications.[1,5,7] However, the use of the single-phase material for high-temperature structural applications is limited by its poor oxidation and ablation resistance, as well as its poor damage tolerance.

The composite approach has been successfully adopted in order to improve the densification, mechanical properties, physical properties, as well as the oxidation and ablation resistance of the ZrB_2 ceramics.[10–21] For example, the addition of 20 vol% fine SiC ($d \approx 0.5\,\mu m$) increased the strength of ZrB_2 to over 1 GPa.[11] The ZrB_2–$MoSi_2$ composites consolidated by spark plasma sintering (SPS) can retain their room temperature strength (~650 MPa) to at least 1200 °C.[18] The addition of $ZrSi_2$ reduced the densification temperature of ZrB_2 to below 1550 °C, as well as increasing its thermal and electrical conductivities.[20,21] Obviously, the mechanical and physical properties of the ZrB_2-based composites are closely linked with the densification process, compositions, starting powder, microstructure, and intergranular second phase. Therefore, it is necessary to understand the relation of performance to processing, compositions, and microstructure in order to produce an ultra-high temperature ZrB_2-based composite with superior performance.

In this article, the densification behaviour, Young's modulus, fracture toughness, flexural strength, thermal and electrical conductivities of the ZrB_2 ceramics and ZrB_2-based composites are reviewed. The emphasis is directed toward presenting recent advances and providing an evaluation of studies of the ZrB_2-based ceramics materials.

2. Densification

Recently, ZrB_2 ceramics and ZrB_2-based composites have been densified by the various methods, including hot pressing (HP), spark plasma sintering (SPS), reactive hot pressing (RHP), and pressureless sintering (PS). Historically, HP has been the dominant method in densification studies. Later, SPS, RHP, and PS processes evolved as the most common densification methods. This section focuses on these four densification processes, as well as on the effects of additives, such as carbides, nitrides and disilicides, on the densification behaviour of zirconium diborides.

2.1. Hot-pressing (HP)

The densification of ZrB_2 powder generally requires very high temperatures,[22] owing to the covalent character of the bonding as well as to its low volume and grain boundary diffusion rates. Typically, HP of ZrB_2 required a temperature of 2100 °C or above and moderate pressure (20–30 MPa),[23–25] or lower temperatures (~1800 °C) and extremely high pressures (>800 MPa).[26,27] These studies[23–27] showed that densification of ZrB_2 is a diffusion-controlled rate process. Results of HP studies on commercially available ZrB_2 powders are summarized in Table 1, which includes details of the starting powders, sintering additives, HP conditions, mixing method and final densities. It has been found that HP of coarse ZrB_2 powder ($d \approx 20\,\mu m$) at 2000 °C with a pressure of 20 MPa achieved only a relative density of ~73%,[24] whereas the relative density of ~91% was obtained for a finer ZrB_2 powder ($d \approx 2.1\,\mu m$) under the same HP conditions.[25] Furthermore, the attrition-milled ZrB_2 powder, with average particle size of $d \leq 0.5\,\mu m$, required HP at 1900 °C and 32 MPa for 45 min to achieve full density.[11] The lower HP temperature was attributed to reduction of starting particle size from microns ($d \approx 2.1\,\mu m$) to submicrons ($d \leq 0.5\,\mu m$) by attrition-milling.

Oxygen impurities (B_2O_3 and ZrO_2) present on the starting powder surfaces have been shown to inhibit densification and to promote grain growth in the non-oxide ceramic systems. A study[28] in TiB_2 suggested that the total oxygen content must be less than 0.5 wt% to achieve full density. Recently, metallic Ni,[29,30] SiC,[10–16,25] Si_3N_4,[31,32] AlN,[33,34] HfN or ZrN,[35,36] have been added to ZrB_2, producing an intergranular secondary phase and/or reducing oxygen content, both of which assists in the densification of ZrB_2. Silicon carbide is the most common additive for ZrB_2 or HfB_2 ceramics. The addition of SiC

Table 1
Starting powder size, hot pressing conditions and final densities of the hot-pressed ZrB_2 ceramics and ZrB_2-based composites with various additives.

Compositions (vol%)	Particles size (μm)		Remarks	Hot-pressing conditions	Final density (%)	References
	ZrB_2	SiC or $MoSi_2$ or $ZrSi_2$				
ZrB_2	20		Ball-milled	2000 °C/20 min/20 MPa	73	24
ZrB_2	2.1		Ball-milled	2000 °C/60 min/30 MPa	91	25
ZrB_2	2		Attrition-milled	1900 °C/45 min/32 MPa	99.8	11
ZrB_2	2		Ball-milled	1650 °C/20 min/60 MPa	71.6	13
ZrB_2	5–10		Ball-milled	1800 °C/60 min/20 MPa	78	37
ZrB_2–2.5 wt% Si_3N_4	0.1–8		Ball-milled	1700 °C/15 min/30 MPa	98	31
ZrB_2–5Si_3N_4	2		Ball-milled	1700 °C/15 min/30 MPa	98	32
ZrB_2–4.6AlN	0.1–8		Ball-milled	1850 °C/30 min/30 MPa	92	33
ZrB_2–15SiC–4.5ZrN	d_{90}- = 4–6		Ball-milled	1900 °C/5 min/50 MPa	99	36
ZrB_2–37.5HfB_2–19.5SiC–3HfN	2		Ball-milled	1900 °C/30 min/50 MPa	>99.9	35
ZrB_2–5.7SiC	2	1.7	Ball-milled	1650 °C/120 min/60 MPa	81.6	13
ZrB_2–22.4SiC	2	1.7	Ball-milled	1650 °C/120 min/60 MPa	97.9	13
ZrB_2–22.4SiC	2	0.04	Ball-milled	1650 °C/120 min/60 MPa	99.6	13
ZrB_2–30SiC	6	10	Attrition-milled	1900 °C/45 min/32 MPa	97.4	14
ZrB_2–30SiC	6	0.7	Attrition-milled	1900 °C/45 min/32 MPa	98.7	14
ZrB_2–16(SiC + C)	5–10	Polycarbosilane (PCS)	Ball-milled	1800 °C/60 min/20 MPa	100	37
ZrB_2–20$MoSi_2$	2	2.8	Ball-milled	1800 °C/5 min/30 MPa	98.1	17
ZrB_2–20$MoSi_2$	2.1	3.1	Ball-milled	1800 °C/30 min/30 MPa	99.8	19
ZrB_2–20$ZrSi_2$	2.1	2.5	Ball-milled	1400 °C/30 min/30 MPa +1550 °C/15 min/30 MPa	99.1	21
ZrB_2–20$MoSi_2$	20	3–5	Ball-milled	2000 °C/20 min/20 MPa	95	24

improved the sinterability, inhibited grain growth and increased the oxidation and ablation resistance of ZrB_2 and HfB_2 ceramics as well.[10–16,25] Monteverde[12] showed that ZrB_2 with 10 vol% ultra-fine SiC ($d_{90} = 0.8$ μm) achieved full density by HP at 1900 °C and 40 MPa for 20 min in vacuo. The attrition-milled ZrB_2–30 vol% SiC mixture powders ($d \approx 0.5$ μm) could be hot-pressed at 1900 °C to a relative density exceeding 97%.[14] Furthermore, the addition of 22.4 vol% nano-sized SiC, with average particles sizes ranging from ~40 nm to 0.6 μm, sharply reduced the HP temperature necessary to achieve full density to 1650 °C (pressed for 120 min at 60 MPa).[13] The improvement of densification upon addition of SiC was attributed to the formation of intergranular liquid phases during hot-pressing, assisting in densification at lower temperatures.[12,13] An early study[29] in 4 wt% Ni-containing ZrB_2 showed that the presence of the liquid phase not only favours ZrB_2 particle rearrangement but also enhances mass transfer kinetics. However, the improvement of densification upon addition of ultra-fine SiC is effective only for a uniformly dispersed SiC–ZrB_2 system.[25] The agglomeration of the ultra-fine SiC particles led to reduced improvement in densification of ZrB_2, even with nano-sized SiC particles.[25] Recently, a polycarbosilane (PCS) was used as a source of SiC and C because the pyrolyzed PCS can crystallize and convert to β-SiC and amorphous C at 1000 °C or above.[37] HP of the PCS-coated ZrB_2 powder required a reduced temperature of 1800 °C (pressed for 60 min at 20 MPa) to achieve a full density when SiC content was ≥16 vol%. For comparison, the ZrB_2 powder without PCS coating was highly porous with a relative density of 78% under the same HP conditions.

Nitrides are other effective additives for improving sinterability or enhancing densification of ZrB_2. The main reason for incorporating nitrides as additives is the propensity of nitrides to consume the oxygen-bearing species on the diboride powder surfaces. The reduction of oxygen results in higher boron activity, which is one of the conditions favouring lattice diffusion and, therefore, densification.[28] The addition of ≥2.5 wt% Si_3N_4 results in almost fully dense ZrB_2 (RD: 98%) after compactions at 1700 °C and 30 MPa for 15 min.[31,32] Some grain boundary phases, including BN, ZrO_2, $ZrSi_2$, and borosilicate glassy phase, were confirmed to be present in pockets at multiple-grains junctions for the ZrB_2-based ceramics with Si_3N_4, the result of a reaction of an oxide impurity with Si_3N_4. That reaction results in elimination or decrease in the oxide impurity on the ZrB_2 particles surfaces, thereby promoting densification.[31,32] Similar to Si_3N_4, the primary effect of an AlN additive is the depletion of the ZrB_2 particles from the outer oxide layer that prevents the formation of highly dense compacts.[33] Compared to AlN and Si_3N_4 additives, the ZrN and HfN showed the unexpected advantage of limiting undesirable secondary phases that eventually become detrimental to high temperature stability. It has been reported that HP of 3 vol% HfN–HfB_2–SiC[35] or 4.5 vol% ZrN–ZrB_2–SiC[36] required 1900 °C for 30 min at a pressure of 40 MPa. The resulting composites showed a fine and homogenous microstructure with secondary phases such as M(C, N), MO_2 (M = Zr and/or Hf) and BN. The formation of the secondary phases during sintering was traced back to the interactions among ZrN or HfN, carbon, and oxides such as B_2O_3 and ZrO_2 or HfO_2. These interactions accelerated the densification of ZrB_2 or HfB_2 ceramics by reducing the oxygen content on the starting powder surfaces. The resulting intergranular secondary phases possess higher refractoriness than those made with AlN or Si_3N_4 additives.

Transition metal disilicides have been found to be an alternative and effective sintering additive because they improve sinterability and increase oxidation resistance of ZrB_2 ceramics as well. In the early 1970s, Kinoshita et al.[24] systematically investigated densification behaviour of ZrB_2-based composites with $MoSi_2$. They found that $MoSi_2$ significantly improved sinterability of ZrB_2 powder and a relative density exceeding 95% was obtained for ≥20 vol% $MoSi_2$-containing ZrB_2 powder at 2000 °C and 20 MPa for 20 min. Recently, it has been reported that HP of the ZrB_2-based ceramics with $MoSi_2$ required only a temperature ≤1800 °C.[17–19] The higher sintering temperature required in the earlier study resulted from larger ZrB_2 ($d \approx 20\,\mu m$) and $MoSi_2$ ($d \approx 5\,\mu m$) particles. More recently, Guo et al.[21] found that addition of 10–40 vol% $ZrSi_2$ could further lower the densification temperature of ZrB_2 to 1550 °C or below. Furthermore, fully dense ZrB_2–$ZrSi_2$ composites with a fine and homogeneous microstructure, using a two-step HP process, which consisted of a first stage at 1400 °C for 30 min and a second stage at 1550 °C for 15 min at a pressure of 30 MPa were obtained. Thus, the disilicides of the transition metals are potential additives for lowering the sintering temperature of the ZrB_2-based ceramics. Consequently, it is possible to further lower the sintering temperature of ZrB_2-based ceramics by selecting appropriate disilicides of transition metals. Improvement of densification, resulting from addition of disilicides, is attributed to two major causes. One is formation of an intergranular Si–O–B liquid phase between $MoSi_2$ or $ZrSi_2$ and ZrB_2 particles due to the interaction of SiO_2 and B_2O_3 that occurs on the surfaces of particles.[38] Another is the ductile deformation of $MoSi_2$ or $ZrSi_2$ particles at high temperature (>800 °C).[39,40] This deformation could force soft $MoSi_2$ or $ZrSi_2$ particles to fill in the voids left by the ZrB_2 skeleton under pressure during sintering, thus improving densification.[19,21]

2.2. Spark plasma sintering (SPS)

SPS is one of the most recent advanced processing techniques developed for densifying ceramic materials.[41,42] Although SPS is similar to HP, in place of indirect heating, the applied electrical field heats the die and the powder compact. One advantage of using SPS is to enhance densification of poorly sinterable ceramics, by simultaneously applying a uniaxial load and a direct or pulsed electric current to a powder compact. Another advantage is that the grain growth of starting materials is restricted, since a considerable shorter sintering time (within minutes) is needed compared to HP or hot isostatic pressing (HIP), thereby retaining the fine and homogeneous grains. Previous investigations[43–45] of compaction of oxide, nitride, and carbide ceramics produced by SPS have shown that the sintering time, heating rate and sintering temperature are the important factors controlling fine-grained microstructure and densification. In particular, the selection of the sintering temperature is critical for the development of the optical microstructure.

Recent studies have shown that SPS enhanced densification and refined microstructure of ZrB_2-based ceramics can be achieved in very short processing cycles.[18,46,47] Table 2 summarizes SPS conditions, final density, and grain size of ZrB_2-based ceramics produced by SPS. Medri et al.[46] showed that 60ZrB_2–30ZrC–10SiC (vol%) composition could be sintered to a relative density of ~96% at 2100 °C and 30 MPa for 2 min. Grain size measurement indicated that the grain growth (maximum grain size: ~3 μm) was inhibited during SPS. Recently, the various ZrB_2–ZrC–SiC compositions could be sintered to the fully dense compacts with fine and homogenous microstructure at 1950 °C and 30 MPa for 2 min, by using the SPS technique.[48] This discrepancy in the sintering temperature is probably associated with starting powder size and SPS conditions. In addition, extending soaking time from 3 min to 5 min can produce fully dense ZrB_2–ZrC–SiC composites at a lower temperature (1900 °C).[34] Furthermore, addition of 5 wt% AlN results in complete densification at 1850 °C and 30 MPa for 5 min, but addition of 5 wt% Si_3N_4 still required a temperature of 1900 °C. The discrepancy in densification temperature due to additions of AlN and Si_3N_4 is likely attributable to a lower onset temperature of densification and a faster shrinking rate for the AlN addition as compared to the Si_3N_4 addition.[34] For the ZrB_2–15 vol% $MoSi_2$,[18] however, the density and grain size measurements of the compacts consolidated at 1750 °C showed that SPS was not superior to HP. Soaking time and total sintering time were noticeably shorter for SPS (7–24 min) than for HP (20–140 min).

Guo et al.[49] systematically investigated the densification behaviour and grain growth of ZrB_2 ceramics produced by SPS. They found that densification and grain size of the sintered ZrB_2 compacts were strongly dependent on the selection of sintering temperature, holding time, as well as the heating rate. It was possible to obtain the almost fully dense ZrB_2 ceramics with a fine and homogeneous microstructure by selecting the appropriate sintering parameters (Fig. 1(a)). Without sintering additives, full density has, historically, been achieved only by HP at temperatures ≥2100 °C.[23,24] Densification and grain growth occurred simultaneously during the sintering. As a result, it was difficult to obtain a full density ZrB_2 compact. SPS of ZrB_2 ceramics required a temperature of 1900 °C, a holding time of 3 min, and a heating rate of 200 °C/min or above. Increasing the sintering temperature to 1950 °C or extending the holding time to 10 min or above, as well as lowering the heating rate below 200 °C/min, led to coarsening of the grain size (typical example, Fig. 1(b)). In addition, SPS has been used for applications in other transition metal diborides, such as HfB_2–SiC,[18] TiB_2–WB_2–CrB_2,[50] TiC–TiB_2,[51] HfB_2–$MoSi_2$,[52] and HfC and HfB_2-based composites with $MoSi_2$ additives.[53] The enhanced densification resulting from SPS was attributable to mass transfer processes, which are significantly enhanced in the process, effectively promoting densification. The mechanism in SPS technique that enhanced densification – mainly whether or how an electric discharge is involved in accelerating the densification and grain growth – is still the subject of intense debate. However, we suggest that enhancement is most probably due to (i) an efficient heat transfer; (ii) the use of comparatively high pressure; (iii) the presence of an electrical field (use of DC pulses); and (iv) the presence of local spark discharges generated between the powders under high-energy electrical pulses.

Table 2
Spark plasma sintering conditions, final density, and grain size of ZrB_2 ceramics and ZrB_2 or HfB_2-based composites produced by an SPS process.

Compositions	Heating rate	SPS conditions	Final density (%)	Grain size (μm)	References
ZrB_2–30ZrC–10SiC (vol%)	100 °C/min	2100 °C/2 min/30 MPa/vacuum	96	~3	46
HfB_2–30SiC (vol%)	100 °C/min	2100 °C/2 min/30 MPa/vacuum	100	2	46
ZrB_2–15$MoSi_2$(vol%)	100 °C/min	1750 °C/7 min/30 MPa/vacuum	97.7	~1.4	18
(15–70)ZrB_2–(15–70)ZrC–(15–50)SiC(mol.%)	~400 °C/min	1950 °C/2 min/50 MPa/Ar	>98	–	48
26.18ZrB_2–59.87ZrC–13.95SiC(wt%)	~400 °C/min	1900 °C/5 min/30 MPa/Ar	99.9	–	34
24.17ZrB_2–56.88ZrC–13.25SiC–5AlN(wt%)	~400 °C/min	1850 °C/5 min/30 MPa/Ar	99.5	–	34
24.17ZrB_2–56.88ZrC–13.25SiC–5AlN(wt%)	~400 °C/min	1900 °C/5 min/30 MPa/Ar	100	–	34
ZrB_2	~300 °C/min	1900 °C/3 min/50 MPa/vacuum	97.6	5.1	49
ZrB_2	~300 °C/min	1900 °C/10 min/50 MPa/vacuum	~80	10	49
ZrB_2	~300 °C/min	1950 °C/3 min/50 MPa/vacuum	98	19	49
HfB_2–(1–9)$MoSi_2$ (vol%)	100 °C/min	1750 °C/3 min/100 MPa/vacuum	>97	1	53
HfC–9$MoSi_2$ (vol%)	100 °C/min	1750 °C/3 min/100 MPa/vacuum	99	0.8	53

2.3. Reactive hot-pressing (RHP)

The use of metallic and ceramic additives during HP could reduce temperature of densification and also inhibit grain growth in ZrB_2 ceramics. However, the significant decreases in the strength at temperatures above 1200 °C that result from softening of intergranular amorphous phase at elevated temperatures has been reported for ZrB_2-based composites with SiC.[18,27,29,30,32] RHP has been identified as a potential route to produce ZrB_2 ceramics with low impurity levels and high density at a lower temperature. There are two processes that occur in RHP, *in situ* reaction of precursor powders and densification, which must be completed simultaneously during heating and subsequent holding.

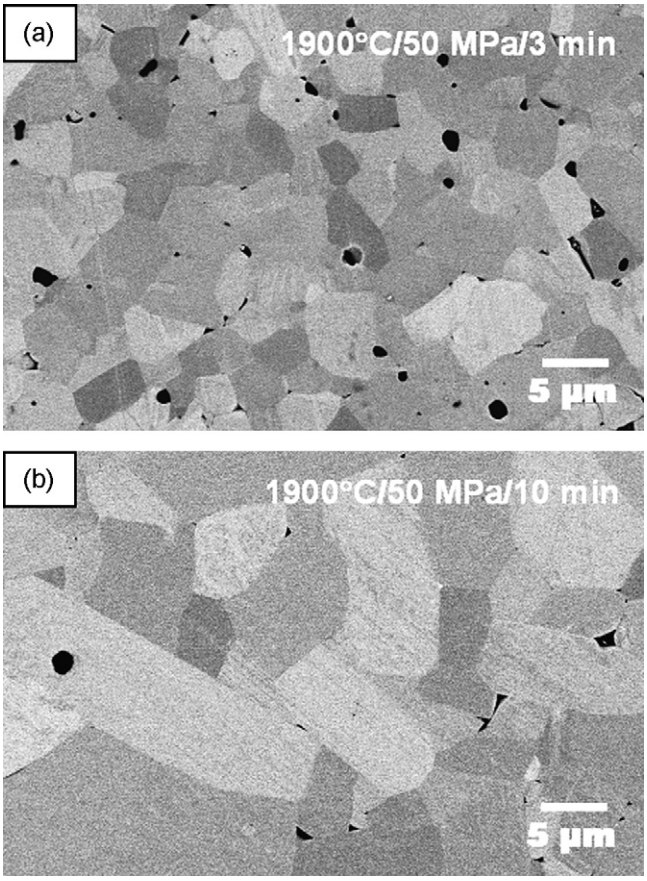

Fig. 1. FE-SEM backscattered electron image of the ZrB_2 ceramics consolidated by SPS at 1900 °C for different holding time of (a) 3 min and (b) 10 min with heating rate of ~200 °C/min under a pressure of 50 MPa in vacuum.[49]

Recently, RHP has been used to produce ZrB_2 and/or HfB_2 dense compacts by using Zr and/or Hf and B precursors as well as to fabricate the ZrB_2-based composites with SiC and/or ZrC by using Zr, Si and B_4C precursors. Table 3 summarizes RHP sintering conditions, precursors, grain size and final density of the ZrB_2 ceramics and ZrB_2-based ceramics fabricated by RHP. Chamberlain et al.[54] have employed slow heating (~1 °C/min) and extended isothermal holds at an extremely low temperature (6 h at 600 °C) to react fine powders of Zr and B without ignition of self-propagating high-temperature synthesis (SHS) reaction. When the samples were heated to 1650 °C in an argon atmosphere, an applied external pressure of 40 MPa produced an almost fully dense, nano-sized ZrB_2 compact. Raising the temperature to 1700 °C increased the density to 99%, however, the ZrB_2 grains were significantly coarsened. The grain size measured in the sample densified at 1800 °C was ~1.5 μm, larger by a factor of ~3 than that at 1650 °C. In contrast, HP of commercially available micron-sized ZrB_2 powders ($d \approx 2.1$ μm) at 2000 °C and 20 MPa for 60 min achieved only a relative density of ~91%,[25] with an average grain size of 6.1 μm. The improvement of densification by RHP was attributed to the formation of nano-sized ZrB_2 particles during the reactive process because the fine crystalline size should enhance the driving force for densification when the densification is driven by minimization of the surface free energy.

Another application of RHP is to produce ZrB_2-based composites with SiC and/or ZrC, using Zr, Si, and B_4C powders as precursors. Zhang et al.[55] used RHP to fabricate ZrB_2-beased composites with SiC, by reacting Zr, Si and B_4C at 1800 °C where the following reaction is thermodynamically favourable:

$$2Zr + Si + B_4C = 2ZrB_2 + SiC \quad (1)$$

The relative density of ~98% was obtained by RHP of Zr, B and B_4C powder mixtures at 1900 °C and 30 MPa for 60 min. Later, Wu et al.[56] also successfully consolidated ZrB_2–SiC–ZrC composites (RD: ~97%) by RHP of Zr, Si

Table 3
Reactive hot-pressing conditions, precursors, grain size and final density of ZrB_2 or HfB_2 ceramics and ZrB_2 or HfB_2-based composites fabricated by a RHP method.

Materials	Precursors	Remarks	HP or SPS Processing conditions	Final density (%)	Grain size (μm)		References
					ZrB_2	SiC	
ZrB_2	Zr, B	Attrition-milled	1650 °C/30 min/40 MPa/Ar (HP)	>95	0.5	–	54
HfB_2	Hf, B	None	1700 °C/10 min/95 MPa/vacuum (SPS)	~98	–	–	59
HfB_2	HfB_2	None	1900 °C/10 min/95 MPa/vacuum (SPS)	~87	–	–	59
ZrB_2–SiC	Zr, Si, B_4C	Ball-milled	1900 °C/60 min/30 MPa/Ar (HP)	96.7	3–10	<3	55
ZrB_2–SiC–ZrC	Zr, Si, B_4C	None	1800 °C/60 min/20 MPa/Ar (HP)	96.8	–	–	56
ZrB_2–SiC	Zr, Si, B_4C	Ball-milled	1450 °C/3 min/30 MPa/vacuum (SPS)	~98.5	<5	<1	60
ZrB_2–SiC	Zr, Si, B_4C	Ball-milled	1890 °C/10 min/30 MPa/vacuum (HP)	100	2	1	57
HfB_2–SiC	Hf, Si, B_4C	Ball-milled	1900 °C/60 min/50 MPa/vacuum (HP)	100	3	1	58

and B_4C powders at 1800 °C and 20 MPa for 60 min in an argon atmosphere. They found that the reactions for producing ZrB_2, ZrC and SiC were not simultaneously induced during the sintering, but in steps. ZrB_2 and ZrC were first formed by the reaction of B_4C with Zr at a low temperature, then SiC was produced by reaction of Si with ZrC and the residual B_4C at a higher temperature. In addition, Zimmermann et al.[57] found that excess B_4C and Si were necessary in the ZrH_2–B_4C–Si system for obtaining ZrB_2–SiC composites without oxide impurity as well as for avoiding grain coarsening during the sintering process. They showed that RHP produced ZrB_2-based ceramics with 27 vol% SiC in the presence of excess B_4C and Si, with an average ZrB_2 grain size of ~2 μm and a SiC particle size of ~1 μm. For comparison, in a stoichiometric ZrH_2, B_4C and Si mixture, the reaction resulted in 25 vol% SiC-containing ZrB_2, accompanied by traces of ZrC and ZrO_2, as a result of deficiency of available boron in the reaction mixture. The grain size appeared to increase from ~2 μm to ~5 μm for the ZrB_2 and from ~1 μm to ~3.5 μm for the SiC. Similarly, RHP is also used to produce the HfB_2-based composites. Monteverde[58] obtained a fully densified HfB_2–22 vol% SiC–6 vol% HfC at 1900 °C and 50 MPa for 60 min through reaction of a mixture of Hf, B_4C and Si powders.

Recently, RHP has also been utilized to produce HfB_2 by reaction of Hf and B powders at a low temperature, by using SPS. An almost fully densified HfB_2 compact was achieved by reacting Hf and B at 1700 °C and 95 MPa for 10 min in vacuo using SPS,[59] instead of HP. For comparison, HfB_2 ceramics produced from commercially available powder could achieved only ~62% and ~87% densities at 1800 °C with 30–85 MPa for 10 min, and at 1900 °C with 80–95 MPa for 10 min,[59] respectively. The reaction between Hf and B occurred at 1100 °C, while the completion of the reaction extended over a relatively wide temperature range.[59] However, the association of the reaction with densification was absent during the reactive sintering. Densification was observed only at a temperature where the conversion to the diboride was complete. In addition, Zhao et al.[60] showed that the reactive sintering of Zr, Si and B_4C precursors could be conducted by SPS. The reactive SPS required a lower temperature of ≥1450 °C with a shorter holding time of 3 min. The resulting composites had a finer and more homogeneous microstructure, compared with that from RHP. Thus, the simultaneous synthesis and consolidation of the Zr, B, or B_4C and Si precursor powders, i.e. reactive sintering, could produce the densified ZrB_2-based composites at a lower temperature by using either HP or SPS, as compared with direct consolidation of commercially available powders.

2.4. Pressureless sintering (PS)

In studies that were conducted in the 1970s and earlier, densification of ZrB_2 ceramics was only accomplished by HP.[5,24,26,27] Because of the extreme pressures required for densification, pressureless sintering of ZrB_2 was considered unlikely or impossible until the late 1980s, when studies of pressureless sintering actually began to show results. Compared with HP, the development of a PS process would enable almost-net-shape processing of ceramic parts with complex geometries using standard powder-processing methods, thus reducing processing costs. Various additives have been used to improve densification of ZrB_2. In general, the additives used can be divided into main two groups: liquid phase formers, and reactive agents. Table 4 summarizes the PS conditions, agents used, grain size and final density of the resulting ZrB_2 ceramics.

Liquid phase formers include refractory metals, such as Ni, Fe, Co, and Mo,[61–63] as well as disilicides of transition metals, such as $MoSi_2$[64,65] and $ZrSi_2$.[20] Cech et al.[61] used Ni, Co, Fe and Re to produce an almost fully densified ZrB_2 at 2000 °C and 2200 °C in vacuo or in an argon atmosphere. They found that addition of ≥2 wt% of metals was required to bring about adequate sintering, because formation and continuous action of a liquid phase occurred only at higher contents of added metals. The additions are more efficient for producing adequate sintering in an argon atmosphere than in vacuo because of loss of the added metals in the vacuum from volatilization. Lattice parameter measurements showed a gradual decrease in the crystal lattice dimensions during sintering, resulting from substitution of zirconium atoms in the ZrB_2 lattice by the atoms of the added metals. Obviously, the mode of action of these metallic additives that influence sintering is associated with an appreciable contraction of the ZrB_2 crystal lattice. Presumably, the contraction of the ZrB_2 crystal lattice affected the surface free energy, and, consequently increased the driving force for densification. A study[63] in TiB_2 with Ni, NiB, and Fe showed that a relative density exceeding 94% was obtained at a temperature ≥1500 °C

Table 4
Pressureless sintering conditions, grain size, and final densities of the pressureless sintered ZrB_2 ceramics with various additives.

Compositions	Remarks	Pressureless sintering conditions	Final density (%)	Grain size (μm)	References
ZrB_2–20 vol% $MoSi_2$	Ball-milled	1850 °C/30 min/Ar	99.1	2–3	65
ZrB_2–4 wt% $MoSi_2$	Ball-milled	2250 °C/120 min/Ar	97.7	3–11	66
ZrB_2–10 vol% $ZrSi_2$	Ball-milled	1650 °C/60 min/Ar	95.7	–	20
ZrB_2–20–40 vol% $ZrSi_2$	Ball-milled	1650 °C/60 min/Ar	>99	–	20
ZrB_2–4 wt% B_4C	Attrition-milled	1850 °C/60 min/vacuum	>98	12	67
ZrB_2–4 wt% B_4C	None	2050 °C/240 min/vacuum	~97	5–6	67
ZrB_2–4 wt% WC	Attrition-milled	2050 °C/240 min/vacuum	95	–	67
ZrB_2–2 vol% WC	Attrition-milled	2150 °C/540 min/He	98	9	71
ZrB_2–1.7 wt% C	Attrition-milled	1900 °C/120 min/Ar	>99	14	70
ZrB_2–4 wt% B_4C	None	2050 °C/120 min/Ar	94	6	69
ZrB_2–4 wt% B_4C	Attrition-milled	1850 °C/120 min/Ar	100	8	69
ZrB_2–4 wt% B_4C–0.5 wt% C	Attrition-milled	1850 °C/120 min/Ar	>99	<4	69
ZrB_2–2 wt% B_4C–0.5 wt% C	None	1900 °C/120 min/Ar	100	4	69

without external pressure, but was accompanied by significantly exaggerated grain growth. The addition of carbon inhibited grain growth, but also significantly increased the porosity. The authors hypothesized that the densification process occurs by redistribution followed by dissolution–reprecipitation in the nickel-rich melt, and that the grain growth was caused by surface diffusion in a titanium-oxide-rich surface layer.[63] In addition, Kislui and Kuzenkova[62] found that with Mo additions up to 15 wt% the energy of activation of the densification process drops below 380 kJ/mol from 680 kJ/mol because Mo was incorporated into a ZrB_2 solid solution. As a result, the addition of Mo activates diffusion processes during sintering, effectively promoting densification. This densification behaviour of Mo is also found in ZrB_2–20 wt% SiC mixture powder that could be sintered without pressure to a relative density exceeding 97.7% at 2250 °C for 120 min when 4 wt% Mo was added.[66] Other studies found that the addition of 20 vol% $MoSi_2$ produced the almost fully densified ZrB_2 at 1850 °C for 30 min without external pressure.[64,65] Furthermore, the additions of ≥20 vol% $ZrSi_2$ further reduced the densification temperature; the full density was obtained at 1650 °C for 60 min.[20]

Differing from the previously mentioned liquid phase formers, reactive agents act as densification aids by reacting with the oxide impurities present on the surface of starting particles (such as ZrO_2 and B_2O_3) which inhibit densification. The main reactive agents used recently include B_4C,[67–69] C,[68–70] and/or WC.[67,71] It was found that the addition of 4 wt% B_4C produces almost the fully dense ZrB_2 compact at 1850 °C for 60 min in vacuo for attrition-milled powder, without externally applied pressure.[67] In contrast, ZrB_2 containing only 4 wt% WC could be sintered to a relative density of ~95% at 2050 °C for 240 min. Chamberlain et al.[71] also showed that the introduction of WC (~2 vol%) allows sintering ZrB_2 powder to an almost fully densified state at 2150 °C for 180 min. They showed that elimination of oxide impurities on ZrB_2 particles surface by the reactions of B_4C or WC with ZrO_2 was the key to densification. The above-mentioned reactions are thermodynamically favourable at a temperature ≥1200 °C for B_4C, but >1500 °C for WC. As a result, the discrepancy in densification temperature between the two agent-doped ZrB_2 ceramics is likely associated with their different onset temperatures for the reactions.

Moreover, grain size measurement showed that excess B_4C restricts the grain growth during sintering. A similar densification and grain growth inhibition effect of B_4C was also reported in ZrB_2-containing B_4C and carbon, either alone or in combination.[69] In addition, the densification effect of B_4C depended on the starting ZrB_2 powder size.[69] ZrB_2 with a particle size of ~2 μm allows sintering to a density of ~95% at 2050 °C for 120 min. For comparison, ZrB_2 could be achieved with full densification at 1850 °C for 60 min when the particle size was reduced to ~0.5 μm by an attrition milling. Furthermore, the densification is more effective for a combination of B_4C and C than for B_4C alone. Using a combination of B_4C and C, the same ZrB_2 powder (~2 μm) could be sintered to almost full density at 1900 °C for 120 min. However, the additional densification effect of carbon does not appear in the reduced particle size ZrB_2 powder (~0.5 μm), which could be sintered to a full density at 1850 °C for 60 min using either B_4C or a combination of B_4C and carbon. Recently, Zhu et al.[70] coated a carbon layer surface of ZrB_2 particles using a phenolic resin as the carbon source. They found that the fully densified ZrB_2 compact could be sintered without pressure at 1900 °C for 120 min, as the carbon content is more than 1.0 wt% in the coated ZrB_2 powders. For comparison, only a relative density of ~70% was obtained for the C-uncoated ZrB_2 powder under the same PS condition.

3. Mechanical behaviours

3.1. Young's modulus

Table 5 summarizes the Young's modulus of ZrB_2 ceramics with and without sintering additives. The Young's modulus ranges from ~350 GPa to 530 GPa, depending on porosity and additives; for a fully densified ZrB_2 without additive, it is equal to 498 GPa.[11] Historic studies have shown the Young's modulus of the fully densified hot-pressed polycrystalline ZrB_2 to be equal to 500 GPa.[72,73] The additions of Ni, AlN, Si_3N_4, B_4C and C affect the Young's modulus of ZrB_2 ceramics; for ZrB_2–4 wt% Ni, it is 496 GPa,[29] higher than that of ZrB_2 of the same density.[71] The Young's modulus of fully densified solids is determined principally by interatomic forces, which decrease sharply with the interatomic distance.[74] The addition of

Table 5
Young's modulus, fracture toughness, and 4-point flexural strength of the ZrB_2 ceramics with and without additives.

Compositions	Process	Grain diameter (μm)	Relative density (%)	Young's modulus (GPa)	Fracture toughness (MPa $m^{1/2}$)	Flexural strength (MPa)	References
ZrB_2	HP	7.7	87	346	2.4	350	32,33
ZrB_2	HP	6.0	99.8	489	3.5	565	11
ZrB_2	HP	6.8	91	417	4.8	457	21
ZrB_2	PS	9	98	454	–	444	71
ZrB_2–4 wt% Ni	HP	5–15	98	496	2.8	371	29
ZrB_2–4.6vol%AlN	HP	4.2	92	407	3.1	580	33
ZrB_2–5 vol% Si_3N_4	HP	3	98	419	3.8	419	32
ZrB_2–4 wt% B_4C	PS	6	94	500	3.3	489	69
ZrB_2–4 wt% B_4C	PS	8	100	530	3.1	370	69
ZrB_2–2 wt% B_4C–1 wt%C	PS	4.1	>99	507	3.5	473	68,69

Ni caused a decrease in the crystal lattice dimensions of ZrB_2, as a result of substitution of Zr atoms in the ZrB_2 lattice by atoms of the added Ni.[61] Therefore, the increase of Young's modulus due to Ni addition is associated with the decrease in the crystal lattice dimensions of ZrB_2. B_4C alone or a combination of B_4C with C also led to an increase in Young's modulus. In contrast, AlN and Si_3N_4 additions led to a lower Young's modulus. The different changes with the additives are associated with the different grain-boundary phase developed between ZrB_2 grains,[32,33,69] which result from the interactions of the additives with impurities on the ZrB_2 particles surfaces, because the grain-boundary phase affects the Young's modulus of ceramics.[34,75]

Fig. 2 is a plot of Young's modulus as a function of the volume fraction of added of SiC, $MoSi_2$ and $ZrSi_2$ to the ZrB_2-based composites. The Young's modulus of the three compositions decreased with amount added, in the order ZrB_2–SiC > ZrB_2–$MoSi_2$ > ZrB_2–$ZrSi_2$, resulting from the maximum modulus value of SiC (~475 GPa[76]), middle value of $MoSi_2$ (~440 GPa[77]), and minimum value of $ZrSi_2$ (~235 GPa[40]). For a fully densified composite, Young's modulus, E_c, may be described by the rule of mixtures[78]

$$E_c = \sum_{i=1}^{n} E_i V_i \quad (2)$$

where E_i is Young's modulus of ith constituent phase, and V_i is volume fraction of ith constituent phase, and n is total number of constituent phases. With E_1 = 500 GPa (ZrB_2),[73] E_2 = 475 GPa (SiC),[76] E_3 = 440 GPa ($MoSi_2$),[77] and E_4 = 235 GPa ($ZrSi_2$),[40] Young's moduli predicted by Eq. (2) are also drawn with three different lines in Fig. 2. A comparison between the measured and predicted values found that Young's modulus of pore-free ZrB_2-based composites obeys the rule of mixtures. For the ZrB_2–10 vol% $ZrSi_2$ composition, the predicted Young's modulus is higher than that measured experimentally, as a result of the presence of pores (RD: 96.6%).

Fig. 3 shows the effect of porosity on Young's modulus measured in ZrB_2–SiC and ZrB_2–ZrC–SiC compositions. It has been found that Young's modulus of the pores-containing ZrB_2-based composites is mostly dominated by the porosity. For ceramic materials, the use of a linear empirical dependence has been recommended. Assuming that the effect of pore structure and shape on Young's modulus is neglected, Young's modulus, E, can be given by[79]

$$E = E_0(1 - \alpha P) \quad (3)$$

where E_0 is Young's modulus of pore-free materials, α is a constant, and P is the volume fraction of porosity in the material.

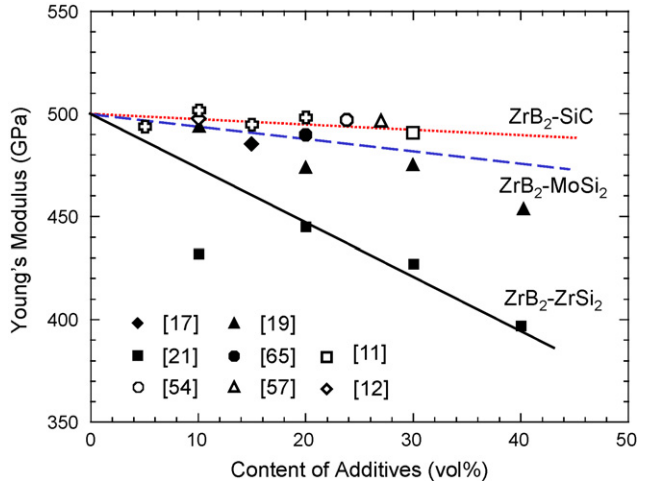

Fig. 2. Young's moduli as a function of additive content for the hot-pressed ZrB_2-based composites with SiC, $MoSi_2$ and $ZrSi_2$ additives.

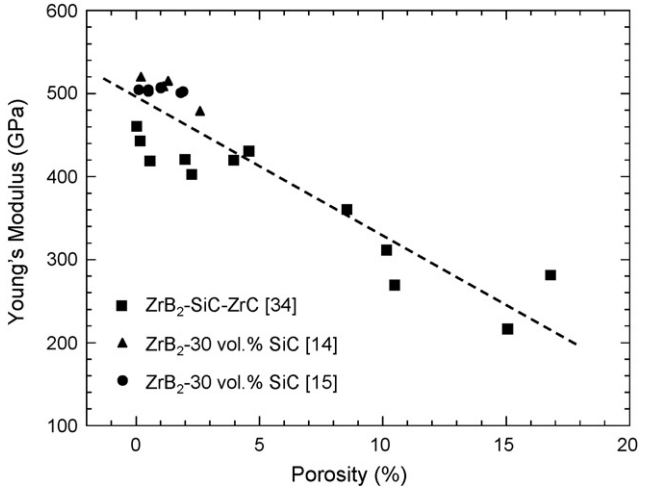

Fig. 3. Young's moduli as a function of porosity for the hot-pressed ZrB_2–30 vol% SiC and spark plasma sintered ZrB_2–ZrC–SiC composites.

The E_0 and α values are obtained from the E–P plots. In addition, the effect of pore structure and shape on Young's modulus have been investigated by other researchers.[80,81] These studies demonstrated that the local elastic moduli decrease when the pore shape changed from spherical to oblate, as a result of the increased stress concentration around the pore. Therefore, the effective elastic modulus measured is lower for the case of non-spherical pores than for the case of spherical pores. Also, it has been found that elastic properties have a different sensitivity to porosity, regardless of pore shape. Bulk modulus is most affected by porosity; Young's modulus is the next most-affected modulus, followed by the shear modulus (which is slightly less sensitive than Young's modulus). In contrast, Poisson's ratio is insensitive to additives as well as to porosity, and it remains almost the constant for the various ZrB_2-based composites.[19,21,34,50]

3.2. Fracture toughness

Fracture toughness of the ZrB_2 ceramics with and without additives is also summarized in Table 5. Fracture toughness was in the range 2.4–4.8 MPa $m^{1/2}$. For the ZrB_2 ceramics with, low fracture toughness, intragranular cracking is common with the cracks propagated across ZrB_2 grains without being deflected along the grain boundaries. For the ZrB_2 with high fracture toughness, intergranular cracking is partially present. In particular, for the case of the fracture toughness of 4.8 MPa $m^{1/2}$,[21] the intergranular cracking was the dominant crack propagation type, with the crack propagated along the grain boundaries (Fig. 4(a)). Thus, large grains and intergranular cracking are required for increasing fracture toughness. Also, the fracture toughness measured is larger in the ZrB_2 with nitrides and/or carbides than with metallic additives. This difference seems to be associated with a larger tensile residual thermal stress in the ZrB_2 ceramics with metallic additives than in the ZrB_2 ceramics with carbide and/or nitride ceramic additives.

Table 6 summarizes the fracture toughness of the ZrB_2-based composites with SiC, $MoSi_2$ and $ZrSi_2$ additives. Rezaie et al.[15] found that the fracture toughness of ZrB_2-based composites with SiC is dominated by the SiC particles size and distribution in the composites. Increased fracture toughness produced by SiC addition is attributed to the crack deflection that occurs near the SiC particles and/or at ZrB_2/SiC interfaces. The interactions of the crack with the microstructure are most likely controlled by the complex residual stress state that develops during cooling from the processing temperature; that in turn is caused by the thermal expansion mismatch between the ZrB_2 and SiC particles. The contribution of crack deflection to increasing fracture toughness depends on the total number of crack deflections and the crack deflection angle, i.e. crack propagation path. Crack deflection is enhanced in larger diameter grains. The increase of fracture toughness that accompanies crack deflection is also associated with the elastic and/or frictional bridging mechanism of grains. Elastic bridging is enhanced in larger diameter grains, while the frictional bridging mechanism is in operation only when crack deflection and grain pullout occur, which is prevalent in smaller diameter grains. Fig. 5 is a plot of fracture toughness as a function of the ratio of ZrB_2 to SiC grain size for ZrB_2–30 vol% SiC composites. *Note that these data are taken in the same test environments in order to avoid the effect of changing test conditions.* It was found that fracture toughness increased with the ratio of ZrB_2 to SiC grain size. This increase of fracture toughness is attributed to the two major causes. One is large ZrB_2 grains enhanced elastic and/or frictional bridging contributions to increasing toughness. Another is small SiC grains increased the number of crack deflections and pullout grains. Therefore, large ZrB_2 grains and/or small SiC grains are required to improve

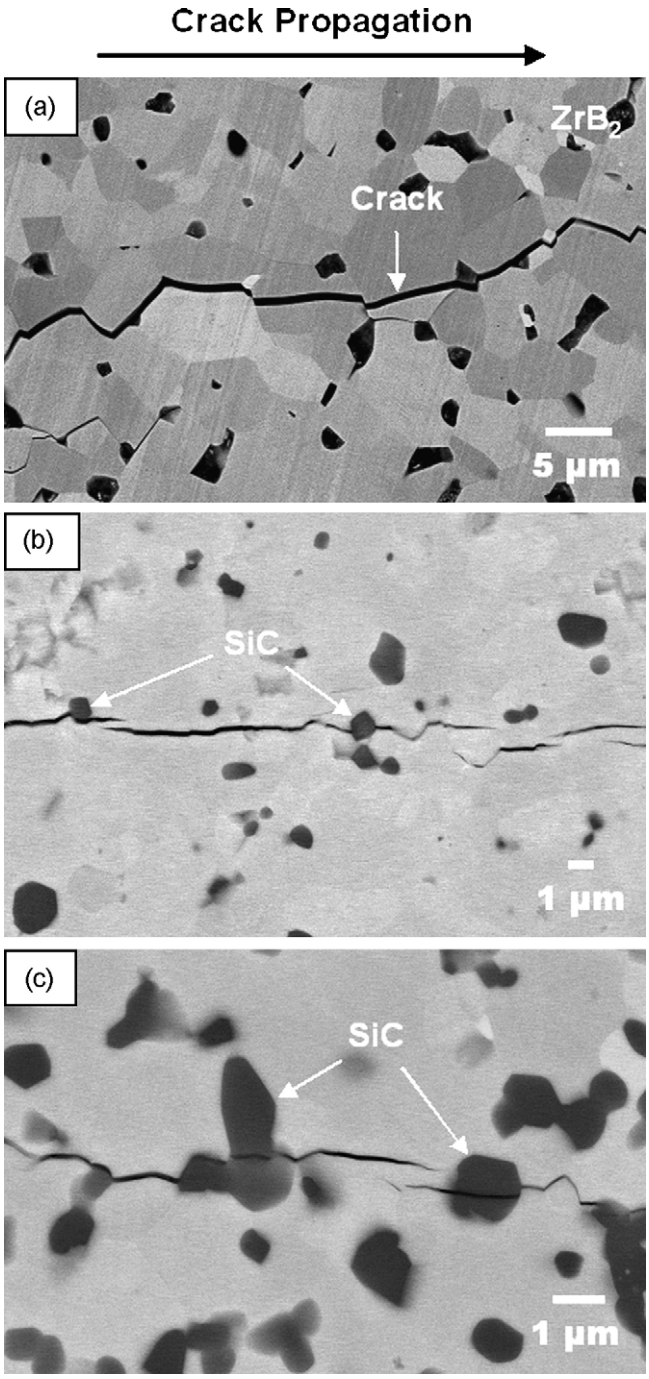

Fig. 4. Typical cracking behaviours for hot-pressed (a) ZrB_2 ceramic with intergranular cracking behaviour, (b) ZrB_2–20 vol% $MoSi_2$–5 vol% SiC, and (c) ZrB_2–20 vol% $MoSi_2$–20 vol% SiC, showing crack deflection at small SiC particles and break of large SiC particles.

Table 6
Young's modulus, Fracture toughness, 4-point flexural strength of the ZrB_2-based composites with SiC, $MoSi_2$ and $ZrSi_2$ additives.

Compositions (vol%)	Relative density (%)	Measured method	Fracture toughness (MPa $m^{1/2}$)	Young's modulus (GPa)	Flexural strength (MPa)	References
ZrB_2–10SiC	93.2	Four-point bending	4.1	450	713	11
ZrB_2–20SiC	99.7	Four-point bending	4.4	466	1003	11
ZrB_2–30SiC	99.4	Four-point bending	5.3	484	1089	11
ZrB_2–30SiC	99.8	Four-point bending	4.6	520	909	14
ZrB_2–30SiC	97.2	Four-point bending	5.5	516	1063	15
ZrB_2–30SiC	99.5	Four-point bending	4.5	505	804	15
ZrB_2–10$MoSi_2$	99.7	Indentation technique	3.7	490	799	19
ZrB_2–20$MoSi_2$	99.8	Indentation technique	2.8	472	749	19
ZrB_2–30$MoSi_2$	99.8	Indentation technique	2.6	473	756	19
ZrB_2–40$MoSi_2$	99.7	Indentation technique	3.1	448	790	19
ZrB_2–20$MoSi_2$–5SiC	100	Indentation technique	3.4	476	862	19
ZrB_2–20$MoSi_2$–10SiC	97.3	Indentation technique	3.4	465	554	19
ZrB_2–20$MoSi_2$–20SiC	94.6	Indentation technique	3.4	461	368	19
ZrB_2–20$MoSi_2$	99.1	Indentation technique	2.3	489	531	65
ZrB_2–10$ZrSi_2$	96.6	Indentation technique	3.8	432	483	21
ZrB_2–20$ZrSi_2$	99.1	Indentation technique	4.4	445	556	21
ZrB_2–30$ZrSi_2$	99.8	Indentation technique	4.4	427	555	21
ZrB_2–40$ZrSi_2$	99.2	Indentation technique	3.9	397	382	21

the toughness of ZrB_2-based ceramics. Recently, a toughness of ~6 MPa $m^{1/2}$ was reached in the ZrB_2–ZrC–SiC system by optimizing the combination of composition with microstructure.[48]

For the ZrB_2–$MoSi_2$ system, fracture toughness is in the range of 2.3–3.7 MPa $m^{1/2}$ and decreased with the content of $MoSi_2$.[19] Differing from the ZrB_2–SiC system, for the ZrB_2–$MoSi_2$ system the crack propagated along ZrB_2 phase boundaries and across the $MoSi_2$ phase,[19] thereby decreasing the toughness of these composites. For comparison, in the ZrB_2–$ZrSi_2$ system the range of fracture toughness values was 3.8–4.4 MPa $m^{1/2}$, tending to improve with $ZrSi_2$ content.[21] This discrepancy between the composite systems seems to be associated with larger ZrB_2 grain size and smaller $ZrSi_2$ grain size in the ZrB_2–$ZrSi_2$ system as compared to the ZrB_2–$MoSi_2$ system.[19,21] Furthermore, it is found that an addition of a small amount of SiC (5 vol%) led to an increase in fracture toughness of the ZrB_2–$MoSi_2$ composites, but the toughness remained almost the constant with further increasing SiC content (≥10 vol%).[19] The crack deflection at the SiC/ZrB_2 interface and the multiple cracking at crack tips contributed to an increase of toughness (Fig. 4(b)). Even with increasing SiC content, crack deflection still occurred only at the smaller individual SiC particles; the crack was across the larger and/or agglomerated SiC particles (Fig. 4(c)). Obviously, the fractured larger SiC particles were not effective in contributing to increase of toughness. The constant toughness with SiC content suggests that most of the added SiC particles were fractured during cracking at high SiC content (≥10 vol%). Thus, a more uniform dispersion of ultrafine SiC particles in the ZrB_2 matrix is important for optimizing fracture toughness.

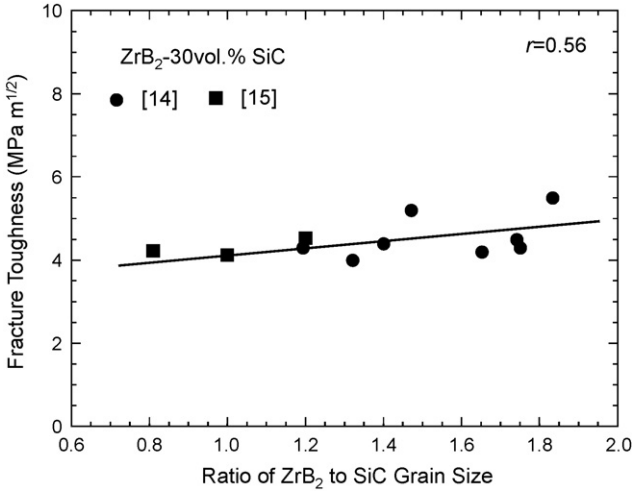

Fig. 5. Plots of fracture toughness as a function of the ratio of ZrB_2 to SiC grain size for the ZrB-based composites with SiC additives.

3.3. Flexural strength

Room-temperature 4-point flexural strengths of the ZrB_2 ceramics with and without additives are also summarized in Table 5. It was found that the flexural strengths range from 350 MPa to 580 MPa, depending on grain size, additives, and on the relative density as well. The hot-pressed ZrB_2 ceramic with AlN showed the highest flexural strength of 580 MPa, although only a relative density of 92% was obtained.[33] For comparison, the flexural strength of ZrB_2 ceramic with Si_3N_4, with ~3 μm grain size and ~98% density, was 419 MPa. This discrepancy is probably associated with an internal tensile stress at the grain boundaries upon cooling from the pressing temperature, which is in turn is caused by the thermal expansion mismatch between the ZrB_2 and grain boundary phase or shrinkage of the intergranular amorphous phase.[82] It is evident that the ZrB_2 ceramic with Ni has the lowest room-temperature flexural strength, resulting from the extremely large thermal expansion mismatch between the ZrB_2 and Ni.[29]

Fig. 6 is a plot of room-temperature 4-point flexural strength as a function of additive content for hot-pressed ZrB_2-based

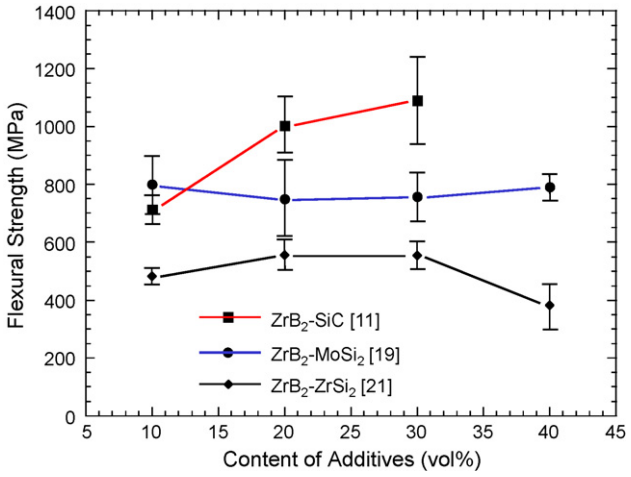

Fig. 6. Plots of room-temperature 4-point flexural strength as a function of additive content for the hot-pressed ZrB_2-based composites with SiC, $MoSi_2$ and $ZrSi_2$ additives.

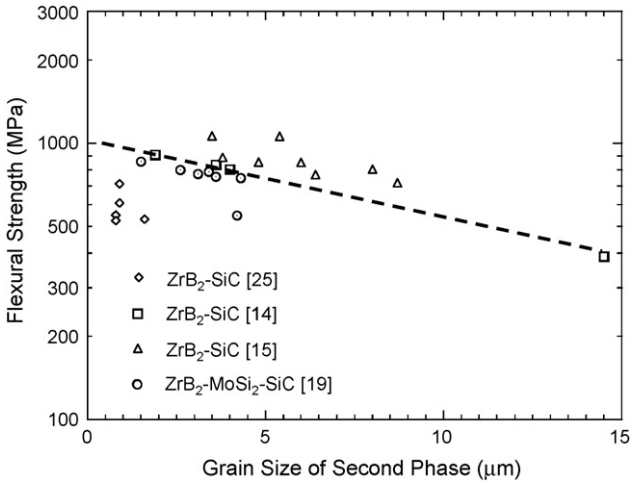

Fig. 7. Plots of room-temperature 4-point flexural strength as a function of grain size of secondary phase for the hot-pressed ZrB_2-based composites with SiC and $MoSi_2$ additives.

composites with SiC, $MoSi_2$ and $ZrSi_2$ additives. Chamberlain et al.[11] showed that the addition of 10, 20 and 30 vol% SiC led to the high room-temperature strengths of ZrB_2, typically ~1000 MPa, with fine ZrB_2 grain microstructure (average grain size: ~2–3 μm). Guo et al.[19] found that the addition of 10–40 vol% $MoSi_2$ increased room-temperature flexural strength of ZrB_2 ceramics to over 700 MPa. Bellosi et al.[18] reported similar results in the 15 vol% $MoSi_2$-containing ZrB_2 ceramics produced by SPS and HP. They found that the flexural strength for $MoSi_2$-containing ZrB_2 composites consolidated both by SPS and HP increased to ~640 MPa and 700 MPa, respectively, corresponding to an average grain size of ~1.4 μm and ~1.8 μm. Comparing both the strength values measured in the ZrB_2–SiC and ZrB_2–$MoSi_2$, it appeared that the strength is higher in the ZrB_2–SiC composites than in the ZrB_2–$MoSi_2$ composites although the grain size of ZrB_2 is larger in the former than in the latter. One exception was a lower strength for a 10 vol% SiC-containing ZrB_2 composite, as a result of the presence of more pores (RD: ~92%). On the other hand, the addition of $ZrSi_2$ improved densification of ZrB_2 ceramics and inhibited grain growth as well (average grain size: ~2–3 μm), but the flexural strength did not increase significantly. Conversely, the addition of 40 vol% $ZrSi_2$ led to a degradation of the strength (~30%). Hence, although ZrB_2 grain size is an important factor affecting the room-temperature flexural strength of ZrB_2-based composites with carbide and disilicides, it is not the limiting factor. A similar conclusion for ZrB_2-based composites with SiC was also reported by Fahrenholtz et al.[5]

Recently, the effects of microstructure and SiC grain size on room-temperature flexural strength were examined in hot-pressed 30 vol% SiC-containing ZrB_2 ceramics by Zhu et al.[14] and Rezaie et al.,[15] both studies showed, based on the linear elastic fracture mechanics, that the critical flaw size correlates strongly with SiC particle size. Both studies concluded that the maximum SiC grain size in the ZrB_2–SiC composites is the strength-limiting factor, and that the strength is not correlated with average ZrB_2 grain size. Similar to ZrB_2–SiC composites, the strong relationship of strength to maximum $MoSi_2$ grain size was also found in ZrB_2–$MoSi_2$ composites (Fig. 7). Thus, it was assumed that the maximum $MoSi_2$ or $ZrSi_2$ grain size dominated the room-temperature strength for ZrB_2-based composites containing $MoSi_2$ or $ZrSi_2$ additives.[19,20] Addition of 5 vol% SiC to ZrB_2–$MoSi_2$ can lead to a further increase of flexural strength.[19] The addition of nano-sized SiC also improved the flexural strength of the ZrB_2–SiC composites before and after oxidation for 10 h at 1400 °C in air (Fig. 8).[25] For comparison, after the oxidation, the strength of 20 vol% micron-sized SiC–ZrB_2 decreased from ~530 MPa before the oxidation to ~500 MPa (Fig. 9).[25] In particular, for single-phase ZrB_2 ceramics, loss of strength reached ~70% after oxidation for 10 h at 1400 °C in air. For the nano-sized SiC–ZrB_2 composites, the increase of strength after oxidation was attributed to the presence of a thin, dense oxide layer on the surface of the post-oxidized samples (Fig. 10(a)). The presence of a thin oxide layer can heal the surface flaws without creating new cracks and defects at the

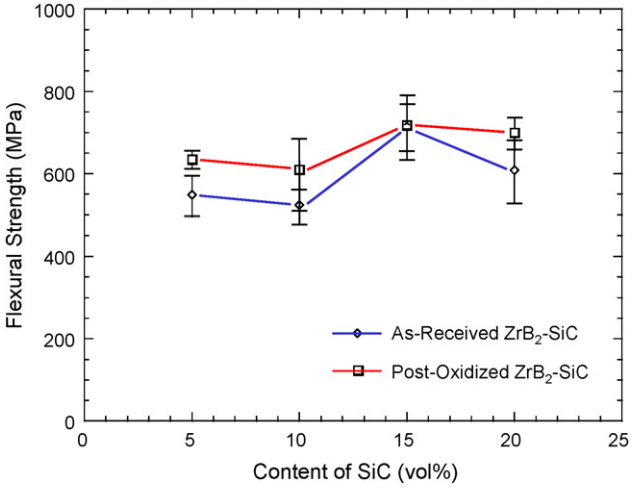

Fig. 8. Effect of thermal exposure at 1400 °C for 10 h in air on room-temperature 4-point flexural strength for the ZrB_2-based composites with nano-sized SiC particles.[25]

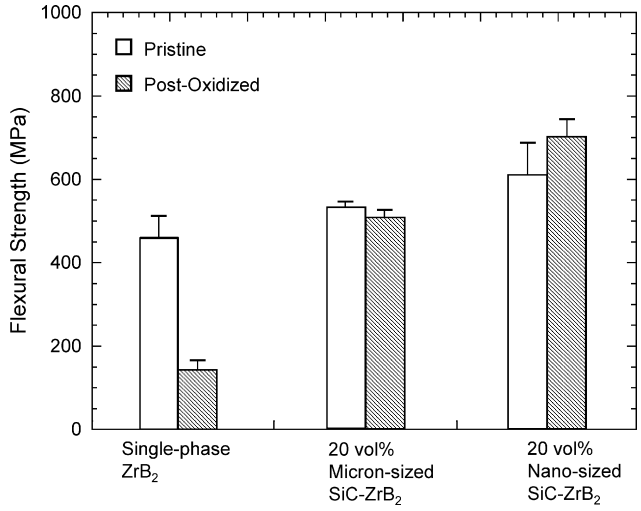

Fig. 9. A comparison of flexural strengths of the single-phase ZrB_2 ceramics, micron- and nano-sized SiC–ZrB_2 composites before and after oxidation at 1400 °C for 10 h in air.[25]

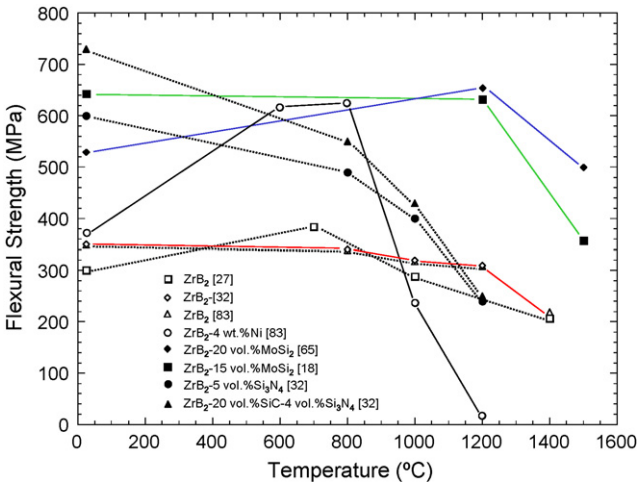

Fig. 11. Plots of 4-point flexural strength as a function of temperature for various the ZrB_2-based composites with various additives.

oxidized surface, and plays a significant role in strength improvement after exposure to an oxidation environment.[83] In contrast, for the micron-sized SiC–ZrB_2 composites, loss of strength due to exposure to high temperatures is attributed to formation of a thicker glassy layer and a defect at the interface between the oxide layer and bulk ZrB_2–SiC composites (indicated by an arrow in Fig. 10(b)).

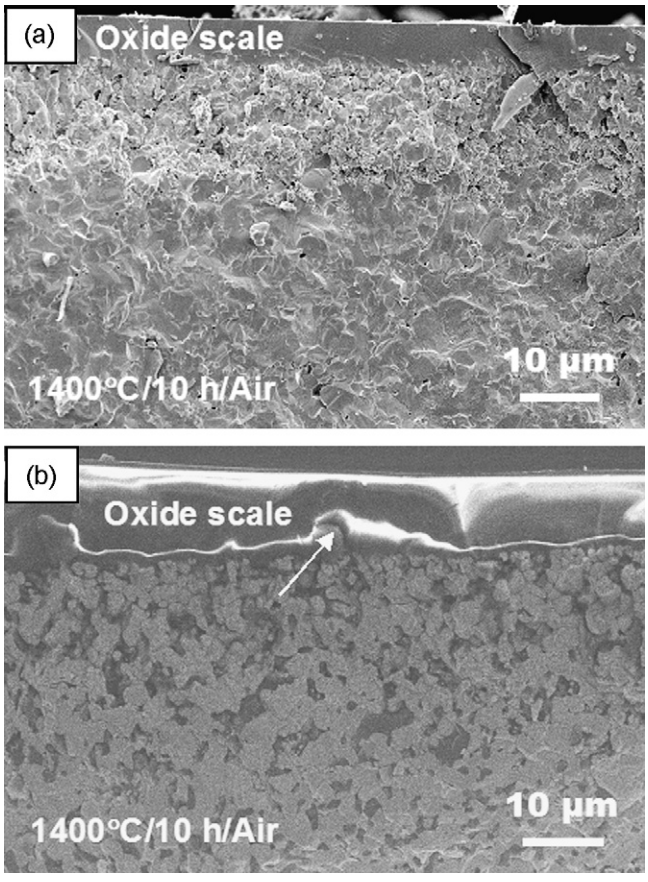

Fig. 10. Typical fracture surfaces of the hot-pressed ZrB_2-based composites with nano- and micron-sized SiC particles after oxidation exposure at 1400 °C for 10 h in air: (a) 20 vol% nano-sized SiC–ZrB_2, and (b) 20 vol% micron-sized SiC–ZrB_2 composite.[25]

Although additives, such as Ni, SiC, and nitrides and disilicides, could reduce the densification temperature of ZrB_2, the strength of the resulting composites is also degraded at high-temperature (Fig. 11), as a result of softening of the intergranular amorphous phase. For the ZrB_2-based ceramics with Ni and Si_3N_4, the strength degraded significantly above 800 °C.[22,30] For the ZrB_2-based ceramics with the Ni additive, in particular, the strength decreased sharply and dropped almost to zero at 1200 °C. For comparison, the ZrB_2-based composites with $MoSi_2$ retained the constant strength at temperatures approaching 1200 °C.[18,65] However, the strength degraded rapidly above 1200 °C, and the degradation was more rapid than in the ZrB_2 ceramics without additive. One exception was the HfB_2–SiC composite produced by SPS, which retained room-temperature strength up to 1500 °C.[18] Although the cause is not completely understood, it is assumed to be closely linked with the minimization of impurities during SPS. Thus, high-temperature strength may be improved by increasing the refractory index of the intergranular phase and minimizing impurities, as well as promoting crystallization of the intergranular amorphous phase.[82]

4. Physical behaviours

Single-phase ZrB_2 and ZrB_2-based composites have high thermal and electrical conductivities among the transition metal carbides, nitrides and diborides. High electrical conductivity allows the fabrication of complex shapes using electrical discharge machining. In addition, high thermal conductivity could improve thermal shock resistance by reducing temperature gradients and thermal stress within the materials. However, the thermophysical and electrical properties of ZrB_2-based composites have not been extensively investigated. This section focuses on recent studies in thermal conductivities and electrical conductivities of ZrB_2 ceramics and ZrB_2-based composites.

Table 7
Thermal conductivity and electrical conductivity of the ZrB_2 ceramics and ZrB_2-based composites with various additives.

Composition (vol%)	Thermal conductivity k ($W\,m^{-1}\,K^{-1}$)	Electrical conductivity σ ($\times 10^4$, $\Omega^{-1}\,cm^{-1}$)	References
ZrB_2	58.2	10.3	8
ZrB_2	56.4	4.5	84
ZrB_2	–	6.7	32,33
ZrB_2–30% SiC	62.1	4.2	84
ZrB_2–4.6AlN	–	4.2	33
ZrB_2–4Ni (wt%)	–	13.5	29
ZrB_2–13B_4C–4Ni (wt%)	–	6.2	29
ZrB_2–5Si_3N_4	–	14.3	32
ZrB_2–20SiC–4Si_3N_4	–	6.7	32
ZrB_2–33.3ZrC–33.3SiC (mol.%)	72.6	1.61	48
ZrB_2–15ZrC–15SiC (mol.%)	85.6	4.52	48
ZrB_2–55ZrC–30SiC (mol.%)	51.8	0.92	48
ZrB_2–15ZrC–30SiC (mol.%)	89.0	3.00	48
ZrB_2–10$MoSi_2$	87.6	8.11	87
ZrB_2–20$MoSi_2$	82.8	7.22	87
ZrB_2–40$MoSi_2$	76.1	7.48	87
ZrB_2–40$MoSi_2$–5SiC	80.8	7.35	87
ZrB_2–40$MoSi_2$–10SiC	84.6	6.04	87
ZrB_2–40$MoSi_2$–20SiC	88.9	4.07	87
ZrB_2–10$ZrSi_2$	98.3	10.7	20
ZrB_2–20$ZrSi_2$	96.8	11.6	20
ZrB_2–30$ZrSi_2$	86.8	11.9	20
ZrB_2–40$ZrSi_2$	74.2	9.6	20

4.1. Thermal conductivity

Table 7 summarizes the thermal conductivities of the ZrB_2 ceramics and ZrB_2-based composites with various additives. The thermal conductivity was generally in the range of 50 $W\,(m\,K)^{-1}$ and 60 $W\,(m\,K)^{-1}$ for the ZrB_2 ceramics.[8,84] Also, an early study[85] of a polycrystalline ZrB_2 showed that thermal conductivity of the ZrB_2 ceramics could achieve a higher value of ~84 $W\,(m\,K)^{-1}$. For single-crystal ZrB_2, the thermal conductivity value was measured to be 140 $W\,(m\,K)^{-1}$ in the basal direction and 100 $W\,(m\,K)^{-1}$ along the c-axis.[86] Thus, the thermal conductivity of the ZrB_2-based composites should be between 50 $W\,(m\,K)^{-1}$ and 140 $W\,(m\,K)^{-1}$. Recently, in the thermal conductivity measurements in various ZrB_2–ZrC–SiC composites consolidated by SPS, it appeared that the conductivity was in the range of 38 $W\,(m\,K)^{-1}$ and 93 $W\,(m\,K)^{-1}$, showing a strong compositional dependence.[48] The thermal conductivity of the ZrB_2–ZrC–SiC composites increased with increasing ZrB_2 as well as SiC content, whereas the conductivities decreased with increasing ZrC content. The compositional dependence of thermal conductivity is also observed in ZrB_2–$ZrSi_2$ and ZrB_2–$MoSi_2$–SiC composite materials.[20,87] It is found that the increase of $MoSi_2$ or $ZrSi_2$ led to a decrease of thermal conductivity of the composites. Conversely, increasing SiC enhanced thermal transport in the ZrB_2–$MoSi_2$–SiC materials; therefore, high thermal conductivity, but the content of added SiC must exceed 5 vol%.

It is known that the thermal conductivity of the composites depend on the thermal conductivity of the components and the interfacial thermal resistance between the components. In the ZrB_2-based composites, the addition of the second phase with higher thermal conductivity than the ZrB_2 phase, such as SiC, led to decreased resistance for the heat flow through the components and their interfaces, thereby increasing thermal conduction. In particular, in the case of the composition with high concentration with SiC, the phase with higher conductivity could form a network-like structure which improved heat capacity, and enhanced heat transport as well, resulting in high thermal conductivity. For comparison, the addition of the second phase with lower thermal conductivity, such as ZrC, $MoSi_2$ and $ZrSi_2$, led to a lower thermal conductivity, probably resulting from the high thermal transport resistance of the second phase, as well as from a higher intergranular thermal resistance.

Fig. 12 is a plot of thermal conductivity as a function of test temperature for the ZrB_2 ceramics and ZrB_2-based composites

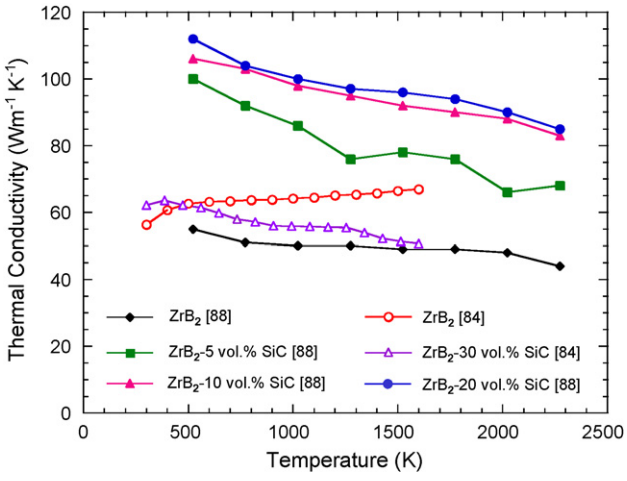

Fig. 12. Plots of thermal conductivity as a function of test temperature for the single-phase ZrB_2 ceramics and ZrB_2-based composites with SiC additives.

with SiC reported in the studies.[84,88] Thermal conductivity was calculated using measured thermal diffusivity determined by the laser flash method, bulk density, and heat capacity. It was found that the thermal conductivity of the ZrB_2 ceramics showed a considerable weak temperature dependence; in particular, the conductivity was almost the constant in the range of ~400 °C to ~1700 °C. In contrast, for the ZrB_2-based composites with SiC, thermal conductivity showed strong temperature dependence. It was found that the thermal conductivity decreased with temperature, regardless of SiC content. Zimmenmann et al.[84] found that the ZrB_2 grain size affects the temperature dependence of the thermal conductivity, and that the conductivity decreased with reduction in grain size. They suggested that the ZrB_2 ceramics and ZrB_2-based composites for use under thermal loading conditions should be examined to determine the optimal grain size to balance the need for thermal transport and strength.

4.2. Electrical conductivity

The ZrB_2 ceramics and ZrB_2-based composites are electrical conductors, which exhibited metallic-like electrical conductivity (Table 7). The electrical conductivity of the pure ZrB_2 ceramics without additives is in the range of 4.5×10^4–10.3×10^4 $(\Omega\,cm)^{-1}$.[8,32,33,89] The discrepancy in the data reported by different authors is probably due to different impurity levels, processing route, and measurement methods. For the ZrB_2 ceramic with additives, the addition of Ni decreased electrical resistance, thereby enhancing electrical conductivity. For comparison, the additions of carbides and nitrides increased electrical resistance, thereby reducing electrical conductivity.[29,33] One exception was an electrical conductivity of the ZrB_2-based ceramics with Si_3N_4 comparable to that of the pure ZrB_2 ceramics although Si_3N_4 is an insulator.[32] In addition, the electrical conductivity of ZrB_2 depended on composition. Rahman et al.[89] showed that the electrical conductivity in the ZrB_2–TiB_2 system decreased with increasing TiB_2, where the zirconium atoms in the ZrB_2 lattice were substituted by the titanium atoms to form a solid solution of $(Zr_{1-x}Ti_x)B_2$ $(0 \le x \le 1)$. As a result, the lower electrical conductivity is due to the higher electrical resistivity of the TiB_2 phase compared to that of the ZrB_2 phase.[89] In addition, they found that the compositional dependence appears to follow linear behaviour at low temperatures (below ~200 °C, Fig. 13), but becomes nonlinear at high temperatures. Furthermore, the temperature dependence of the electrical resistivity of the ZrB_2 ceramics and ZrB_2-based composites are similar to that of metals; the resistivity increased linearly with temperature, examples of which are shown in Fig. 14. However, the addition of SiC led to an increase of electrical resistivity of ZrB_2 ceramics; the increase was enlarged significantly with increasing temperature. The thermal coefficient of electroresistance (TCR), β, was given by[90]

$$\beta = \frac{1}{\rho_{298}} \frac{d\rho(T)}{dT} \quad (4)$$

where ρ_{298} is the room temperature electrical resistivity, and T is the absolute temperature. The TCR values were found to be in the range of 1.0×10^{-3} K^{-1} to 6.4×10^{-3} K^{-1} for ZrB_2,[84,85,89,90] and the TCR is approximately 1.4×10^{-3} K^{-1} for a solid solution of $(Zr_{1-x}Ti_x)B_2$ $(0 \le x \le 1)$.[89] The addition of SiC increased the TCR of ZrB_2 ceramics. Tye and Clougherty[85] showed that the TCR value was 4.8×10^{-3} K^{-1} for ZrB_2–20 vol% SiC composites, whereas Zimmenmann et al.[84] reported that the measured TCR value was ~2.5×10^{-3} K^{-1} for ZrB_2–30 vol% SiC.

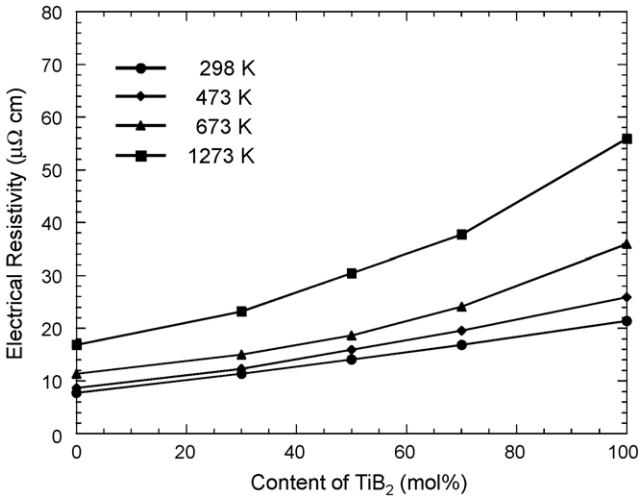

Fig. 13. Plots of electrical resistance as a function of content of TiB_2 for the ZrB_2–TiB_2 composites at various temperatures.[89]

Also, Jimbou et al.[91,93] and Takahashi et al.[92] found that an electrical percolation threshold is observed in the ZrB_2–SiC system. The electrical resistivity of ZrB_2–SiC composites sharply increased with SiC content over 70 vol%, as shown in Fig. 15. Presumably, below the critical content of SiC, the network-like structure formed by the ZrB_2 phase with high-electrical conductivity provides an electrical path with lower resistance, thereby retaining high electrical conductivity. The electrical resistivity values measured in the ZrB_2–SiC composition (SiC content: <70 vol%) have below an order of 6 in magnitude, compared with that of pure SiC. Furthermore, the grain diameter and

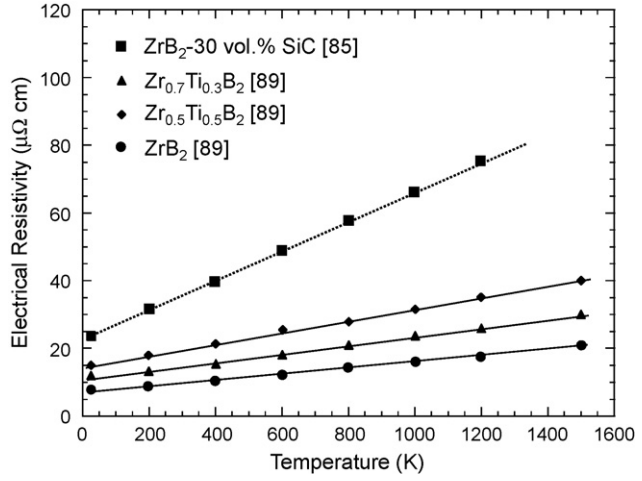

Fig. 14. Plots of electrical resistivity as a function of temperature for the ZrB_2 ceramics and ZrB_2–30 vol% SiC composite.

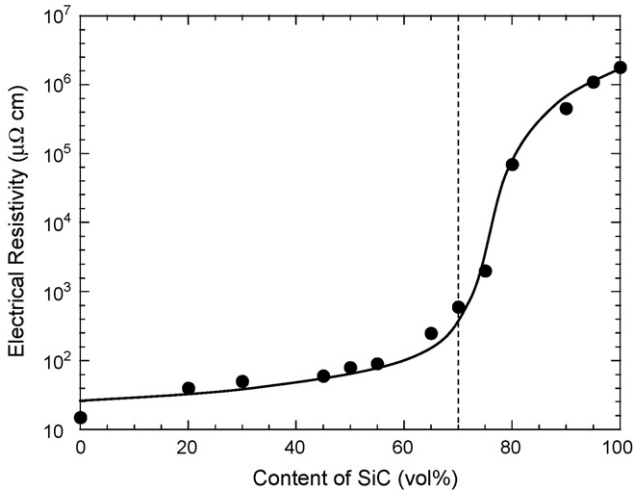

Fig. 15. Plots of electrical resistivity as a function of SiC content for the ZrB_2-based composites with SiC additives.[91–93]

aspect ratio of ZrB_2 affect the electrical conductivity.[92,93] Larger grain diameter and high aspect ratio of ZrB_2 particles led to formation of a network of ZrB_2 particles in the composite, therefore resulting in high electrical conductivity. Recently, ZrC was incorporated in the ZrB_2–SiC system,[48] the electrical conductivity of the resulting ZrC–ZrB_2–SiC composites was in the range of 0.92×10^4–4.52×10^4 $(\Omega\,cm)^{-1}$, and it decreased with increasing ZrC and/or SiC content.

Moreover, for the ZrB_2–$MoSi_2$ composite (Table 7), the electrical conductivity decreased with $MoSi_2$ addition.[87] The additions of 10 and 20 vol% SiC lowered the electrical conductivity of the ZrB_2–$MoSi_2$ composites further. However, an addition 5 vol% SiC was ineffective in lowering electrical conductivity. Although the additions of $MoSi_2$ and SiC decreased electrical conductivity of ZrB_2 materials, the electrical conductivities of the ZrB_2–$MoSi_2$–SiC composites are in the range characteristic of conductors. For ZrB_2–$ZrSi_2$ composites (Table 7),[20] the electrical conductivity was almost constant with the additions of ≤30 vol%, the conductivity decreased with further addition of $ZrSi_2$. The electrical conductivity of the composites is in the range of 9.6×10^4–11.9×10^4 $(\Omega\,cm)^{-1}$. Thus, the addition of 30 vol% $ZrSi_2$ is critical for retaining the high electrical conductivity of ZrB_2 ceramic.

5. Summary remarks

This paper reviews the densification, Young's modulus, fracture toughness, flexural strength, thermal and electrical conductivities of ZrB_2-based composites. The concluding remarks are follows.

(1) Hot-pressing (HP) is the most common densification method for ZrB_2-based ceramics in historic studies. The additions of metals, carbides, nitrides, and disilicides, as well as reducing particle sizes, improved sinterability and lowered the densification temperature. Reactive hot pressing (RHP) of Zr, B, or B_4C and Si precursors could produce the ZrB_2 and ZrB_2-based composites with SiC and/or ZrC at lower temperatures, compared with HP. Pressureless sintering of ZrB_2-based composites was possible by addition of B_4C, C, $MoSi_2$ and $ZrSi_2$. Spark plasma sintering (SPS) could densify various compositions of ZrB_2-based composites at a lower temperature and very short soaking time, compared to the HP, RHP and PS methods.

(2) Young's modulus of the ZrB_2-based ceramics was in the range of 300–500 GPa, strongly dependent on additives and porosity. Young's modulus of porosity-free ZrB_2-based composites could be predicted by the rule of mixtures.

(3) Fracture toughness of the ZrB_2-based ceramics was in the range of 2–6 MPa $m^{1/2}$. The fracture toughness is dominated by secondary phase particle size and distribution. Larger ZrB_2 grain and small second phase grain could increase fracture toughness, as a result of crack deflection at the grain-boundary interfaces. This is associated with the complex residual stress within grains and at the grain-boundaries.

(4) Flexural strength of the ZrB_2-based ceramics was significantly increased by additions of second phase particles. The secondary phase particle size and distribution governed the room-temperature strength. The addition of fine SiC particles showed the highest room temperature strength. In addition, the addition of nano-sized SiC improved strength of ZrB_2–SiC composites after oxidation of 10 h at 1400 °C in air, while the strength of ZrB_2-based composites with micron-sized SiC decreased. Further improvement in strength may be achieved through a more uniform dispersion of nano-sized particles in ZrB_2 matrix.

(5) Thermal conductivity of the ZrB_2-based ceramics was in the range of 30–140 W $(m\,K)^{-1}$, depending on composition as well as grain size. The addition of SiC increased thermal conductivity, whereas the additions of $MoSi_2$ and $ZrSi_2$ decreased the conductivity. The thermal conductivity remained almost constant with temperature for the ZrB_2 ceramics in the range of 400–1700 °C, whereas the conductivity of ZrB_2-based composite with SiC decreased with temperature.

(6) Electrical conductivity of the ZrB_2-based composites was in the range of $\sim 1 \times 10^4$ $(\Omega\,cm)^{-1}$ to 12×10^4 $(\Omega\,cm)^{-1}$, depending on composition. The additions of SiC and $MoSi_2$ led to decrease in the electrical conductivity, while the addition of $ZrSi_2$ (≤30 vol%) had not the noticeable effect on the electrical conductivity.

References

1. Upadhya, K., Yang, J.-M. and Hoffmann, W. P., Materials for ultrahigh temperature structural applications. *Am. Ceram. Soc. Bull.*, 1997, **76**(12), 51–56.
2. Berton, B., Bacos, M. P., Demange, D. and Lahaye, J., High-temperature oxidation of silicon carbide in simulated atmospheric re-entry conditions. *J. Mater. Sci.*, 1992, **27**, 3206–3210.
3. Scott, H. G., Phase relationships in the zirconia–yttria system. *J. Mater. Sci.*, 1975, **10**, 1527–1535.
4. Kajihara, K., Yoshizawa, Y. and Sakuma, T., The enhancement of superplastic flow in tetragonal zirconia polycrystals with SiO_2-doping. *Acta Metall. Mater.*, 1995, **43**(3), 1235–1242.

5. Fahrenholtz, W. G., Hilmas, G. E., Talmy, I. G. and Zaykoski, J. A., Refractory diborides of zirconium and hafnium. *J. Am. Ceram. Soc.*, 2007, **90**(5), 1347–1364.
6. Mroz, C., Zirconium diboride. *Am. Ceram. Soc. Bull.*, 1994, **73**(6), 141–142.
7. Brown, A. S., Hypersonic designs with a sharp edge. *Aerospace Am.*, 1997, **35**(9), 20–21.
8. Kuwabara, K., Some characteristics and applications of ZrB_2 ceramics. *Bull. Ceram. Soc. Jpn.*, 2002, **37**(4), 267–271.
9. Norasetthekul, S., Eubank, P. T., Bradley, W. L., Bozkurt, B. and Stucker, B., Use of zirconium diboride-copper as an electrode in plasma applications. *J. Mater. Sci.*, 1999, **34**(6), 1261–1270.
10. Trip, W. C., Davis, H. H. and Graham, H. C., Effect of an SiC addition on the oxidation of ZrB_2. *Am. Ceram. Soc. Bull.*, 1973, **52**, 612–616.
11. Chamberlain, A. L., Fahrenholtz, W. G., Hilmas, G. E. and Ellerby, D. T., High-strength zirconium diboride-based ceramics. *J. Am. Ceram. Soc.*, 2004, **87**(6), 1170–1172.
12. Monteverde, F., Beneficial effects of an ultra-fine α–SiC incorporation on the sinterability and mechanical properties of ZrB_2. *Appl. Phys. A*, 2006, **82**, 329–337.
13. Hwang, S. S., Vasiliev, A. L. and Padture, N. P., Improved processing and oxidation-resistance of ZrB_2 ultra-high temperature ceramics containing SiC nanodispersoids. *Mater. Sci. Eng. A*, 2007, **A464**, 216–224.
14. Zhu, S., Fahrenholtz, W. G. and Hilmas, G. E., Influence of silicon carbide particle size on the microstructure and mechanical properties of zirconium diboride-silicon carbide ceramics. *J. Euro. Ceram. Soc.*, 2007, **27**, 2077–2083.
15. Rezaie, A., Fahrenholtz, W. G. and Hilmas, G. E., Effect of hot-pressing time and temperature on the microstructure and mechanical properties of ZrB_2–SiC. *J. Mater. Sci.*, 2007, **42**, 2735–2744.
16. Clougherty, E. V., Pober, R. L. and Kaufman, L., Synthesis of oxidation resistance metal diboride composites. *Trans. TMS AIME*, 1968, **242**(6), 1077–1082.
17. Sciti, D., Monteverde, F., Guicciardi, S., Pezzotti, G. and Bellosi, A., Microstructure and mechanical properties of ZrB_2-$MoSi_2$ ceramic composites produced by different sintering techniques. *Mater. Sci. Eng. A*, 2006, **A434**, 303–309.
18. Bellosi, A., Monteverde, F. and Sciti, D., Fast densification of ultra-high-temperature ceramics by spark plasma sintering. *Int. J. Appl. Ceram. Technol.*, 2006, **3**(1), 32–40.
19. Guo, S. Q., Nishimura, T., Mizuguchi, T. and Kagawa, Y., Mechanical properties of hot-pressed ZrB_2-$MoSi_2$-SiC composites. *J. Eur. Ceram. Soc.*, 2008, **28**(9), 1891–1898.
20. Guo, S. Q., Kagawa, Y., Nishimura, T. and Tanaka, H., Pressureless-sintering and physical properties of ZrB_2-based composites with $ZrSi_2$ additive. *Scripta Mater.*, 2008, **58**(7), 579–582.
21. Guo, S. Q., Kagawa, Y. and Nishimura, T., Mechanical behavior of two-step hot-pressed ZrB2-based composites with $ZrSi_2$. *J. Eur. Ceram. Soc.*, 2009, **29**(4), 787–794.
22. Pastor, M., Metallic borides: preparation of solid bodies, sintering methods and properties of solid bodies. In *Boron and Refractory Borides*, ed. V. I. Matkovich. Springer, New York, 1977, pp. 457–493.
23. Meeson, G. A. and Gorbunow, A. F., Activated sintering of zirconium boride. *Inorg. Mater.*, 1968, **4**, 267–270.
24. Kinoshita, M., Kose, S. and Hamano, Y., Hot-pressing of zirconium diboride-molybdenum disilicide mixtures. *Yogyo-Kyokai-Shi*, 1970, **78**(2), 32–41.
25. Guo, S. Q., Yang, J.-M., Tanaka, H. and Kagawa, Y., Effect of thermal exposure on strength of ZrB_2-based composites with nano-sized SiC particles. *Comp. Sci. Technol.*, 2008, **68**(14), 3033–3040.
26. Kalish, D. and Clougherty, E. V., Densification mechanisms in high-pressure hot-pressing of HfB_2. *J. Am. Ceram. Soc.*, 1969, **52**(1), 26–30.
27. Kalish, D., Clougherty, E. V. and Kreder, K., Strength, fracture mode, and thermal stress resistance of HfB_2 and ZrB_2. *J. Am. Ceram. Soc.*, 1969, **52**(1), 30–36.
28. Baik, S. and Becher, P. F., Effect of oxygen contamination on densification of TiB_2. *J. Am. Ceram. Soc.*, 1987, **70**(8), 527–530.
29. Monteverde, F., Bellosi, A. and Guicciardi, S., Processing and properties of zirconium diboride-based composites. *J. Eur. Ceram. Soc.*, 2002, **22**, 279–288.
30. Melendez-Martinez, J. J., Dominguez-Rodriguez, A., Monteverde, F., Melandri, C. and de Portu, G., Characterization and high temperature mechanical properties of zirconium boride-based materials. *J. Eur. Ceram. Soc.*, 2002, **22**, 2543–2549.
31. Monteverde, F. and Bellosi, A., Effect of the addition of silicon nitride on sintering behavior and microstructure of zirconium diboride. *Scripta Mater.*, 2002, **46**, 223–228.
32. Monteverde, F., Guicciardi, S. and Bellosi, A., Advances in microstructure and mechanical properties of zirconium diboride based ceramics. *Mater. Sci. Eng. A*, 2003, **A346**, 310–319.
33. Monteverde, F. and Bellosi, A., Beneficial effects of AlN as sintering aid on microstructure and mechanical properties of hot-pressed ZrB_2. *Adv. Eng. Mater.*, 2003, **5**(7), 508–512.
34. Guo, S. Q., Kagawa, Y., Nishimura, T. and Tanaka, H., Elastic properties of spark plasma sintered (SPSed) ZrB_2–ZrC–SiC composites. *Ceram. Int.*, 2008, **34**(8), 1811–1817.
35. Monteverde, F. and Bellosi, A., Efficacy of HfN as sintering aid in the manufacture of ultra-high-temperature metal diborides-matrix ceramics. *J. Mater. Res.*, 2004, **19**(12), 3576–3585.
36. Monteverde, F. and Bellosi, A., Development and characterization of metal-diboride-based composites toughened with ultra-fine SiC particulates. *Solid State Sci.*, 2005, **7**, 622–630.
37. Zhou, X.-J., Zhang, G.-J., Li, Y.-G., Kan, Y.-M. and Wang, P.-L., Hot-pressed ZrB_2–SiC–C ultra-high temperature ceramics with polycarbosilane as a precursor. *Mater. Lett.*, 2007, **61**, 960–963.
38. Rockett, T. J. and Foster, W. R., Phase relations in the system boron oxide-silica. *J. Am. Ceram. Soc.*, 1965, **48**(2), 75–80.
39. Jeng, Y.-L. and Lavernia, E. J., Review: processing of molybdenum disilicide. *J. Mater. Sci.*, 1994, **29**, 2557–2571.
40. Rosenkranz, R. and Frommeyer, G., Microstructures and properties of the refractory compounds $TiSi_2$ and $ZrSi_2$. *Z. Metalkd.*, 1992, **83**(9), 685–689.
41. Tokida, M., Trends in advanced spark plasma sintering system and technology. *J. Soc. Powder Technol. Jpn.*, 1993, **30**(11), 790–804.
42. Nygren, M. and Shen, Z., On the preparation of bio-, nano- and structural ceramics and composites by spark plasma sintering. *Solid State Sci.*, 2003, **5**, 125–131.
43. Shen, Z., Johnsson, M., Zhao, Z. and Nygren, M., Spark plasma sintering of alumina. *J. Am. Ceram. Soc.*, 2002, **85**(8), 1921–1927.
44. Khor, K. A., Cheng, K. H., Yu, L. G. and Boey, F., Thermal conductivity and dielectric constant of spark plasma sintered aluminum nitride. *Mater. Sci. Eng. A*, 2003, **A347**, 300–305.
45. Guillard, F., Allemand, A., Luetic, J. D. and Galy, J., Densification of SiC by SPS-effects of times, temperature and pressure. *J. Eur. Ceram. Soc.*, 2007, **27**, 2725–2728.
46. Medri, V., Monteverde, F., Balbo, A. and Bellosi, A., Comparison of ZrB_2-ZrC-SiC composites fabricated by spark plasma sintering and hot-pressing. *Adv. Eng. Mater.*, 2005, **7**(3), 159–163.
47. Venkateswaran, T., Basu, B., Raju, G. B. and Kim, D.-Y., Densification and properties of transition metal borides-based ceramics via spark plasma sintering. *J. Eur. Ceram. Soc.*, 2006, **26**, 2431–2440.
48. Guo, S. Q., Kagawa, Y., Nishimura, T., Chung, D. and Yang, J.-M., Mechanical and physical behavior of spark plasma sintered ZrC–ZrB_2–SiC multiphase composites. *J. Eur. Ceram. Soc.*, 2008, **28**, 1279–1285.
49. Guo, S. Q., Nishimura, T., Kagawa, Y. and Yang, J.-M., Spark plasma sintering of zirconium diborides. *J. Am. Ceram. Soc.*, 2008, **91**(9), 2848–2855.
50. Kaga, H., Heian, E. M., Munir, Z. A., Schmalzried, C. and Telle, R., Synthesis of hard materials by field activation: the synthesis of solid solutions and composites in the TiB_2-WB_2-CrB_2 system. *J. Am. Ceram. Soc.*, 2001, **84**(12), 2764–2770.
51. Locci, A. M., Orru, R., Cao, G. and Munir, Z. A., Simultaneous spark plasma synthesis and densification of TiC–TiB_2 composites. *J. Am. Ceram. Soc.*, 2006, **89**(3), 848–855.
52. Sciti, D., Silvestroni, L. and Bellosi, A., Fabrication and properties of HfB_2-$MoSi_2$ composites produced by hot pressing and spark plasma sintering. *J. Mater. Res.*, 2006, **21**(6), 1460–1466.

53. Sciti, D., Guicciardi, S. and Nygren, M., Densification and mechanical behavior of HfC and HfB_2 fabricated by spark plasma sintering. *J. Am. Ceram. Soc.*, 2008, **91**(5), 1433–1440.
54. Chamberlain, A. L., Fahrenholtz, W. G. and Hilmas, G. E., Low-temperature densification of zirconium diboride ceramics by reactive hot pressing. *J. Am. Ceram. Soc.*, 2006, **89**(12), 3638–3645.
55. Zhang, G.-J., Deng, Z.-Y., Kondo, N., Yang, J.-F. and Ohji, T., Reactive hot pressing of ZrB_2-SiC composites. *J. Am. Ceram. Soc.*, 2000, **83**(9), 2330–2332.
56. Wu, W.-W., Zhang, G.-J., Kan, Y.-M. and Wang, P.-L., Reactive hot pressing of ZrB_2-SiC-ZrC ultra high-temperature ceramics at 1800 °C. *J. Am. Ceram. Soc.*, 2006, **89**(9), 2967–2969.
57. Zimmermann, J. W., Hilmas, G. E., Fahrenholtz, W. G., Monteverde, F. and Bellosi, A., Fabrication and properties of reactively hot pressed ZrB_2-SiC ceramics. *J. Eur. Ceram. Soc.*, 2007, **27**, 2729–2736.
58. Monteverde, F., Progress in the fabrication of ultra-high-temperature ceramics: in situ synthesis, microstructure and properties of a reactive hot-pressed HfB_2-SiC composite. *Compos. Sci. Technol.*, 2005, **65**, 1869–1879.
59. Anselmi-Tamburini, U., Kodera, Y., Gasch, M., Unuvar, C., Munir, Z. A., Ohyanagi, M. and Johnson, S. M., Synthesis and characterization of dense ultra-high temperature thermal protection materials produced by field activation through spark plasma sintering (SPS): 1. Hafnium diboride. *J. Mater. Sci.*, 2006, **41**, 3097–3104.
60. Zhao, Y., Wang, L.-J., Zhang, G.-J., Jiang, W. and Chen, L.-D., Preparation and microstructure of a ZrB_2-SiC composite fabricated by the spark plasma sintering-reactive synthesis (SPS-RS) method. *J. Am. Ceram. Soc.*, 2007, **90**(12), 4040–4042.
61. Cech, B., Oliverius, P. and Sejbal, J., Sintering of zirconium boride with activating additions. *Powder Metall.*, 1965, **8**(15), 142–151.
62. Kislui, P. S. and Kuzenkova, M. A., Regularities of sintering of zirconium diboride-molybdenum alloys. *Sov. Powder Metall. Met. Ceram.*, 1966, **5**, 360–365.
63. Einarsrud, M.-A., Hagen, E., Pettersen, G. and Grande, T., Pressureless sintering of titanium diboride with nickel, nickel boride, and iron additives. *J. Am. Ceram. Soc.*, 1997, **80**(12), 3013–3020.
64. Sciti, D., Brach, M. and Bellosi, A., Oxidation behavior of a pressureless sintered ZrB_2-$MoSi_2$ ceramic composites. *J. Mater. Res.*, 2005, **20**(4), 922–930.
65. Sciti, D., Guicciardi, S., Bellosi, A. and Pezzotti, G., Properties of a pressureless-sintered ZrB_2-$MoSi_2$ ceramic composite. *J. Am. Ceram. Soc.*, 2006, **89**(7), 2320–2322.
66. Yan, Y., Huang, Z., Dong, S. and Jiang, D., Pressureless sintering of high-density ZrB_2-SiC ceramic composites. *J. Am. Ceram. Soc.*, 2006, **89**(11), 3589–3592.
67. Zhang, S. C., Hilmas, G. E. and Fahrenholtz, W. G., Pressureless densification of zirconium diboride with boron carbide additives. *J. Am. Ceram. Soc.*, 2006, **89**(5), 1544–1550.
68. Zhu, S., Fahrenholtz, W. G., Hilmas, G. E. and Zhang, S. C., Pressureless sintering of zirconium diboride using boron carbide and carbon additions. *J. Am. Ceram. Soc.*, 2007, **90**(11), 3660–3663.
69. Fahrenholtz, W. G., Hilmas, G. E., Zhang, S. C. and Zhu, S., Pressureless sintering of zirconium diboride: particle size and additive effects. *J. Am. Ceram. Soc.*, 2008, **91**(5), 1398–1404.
70. Zhu, S., Fahrenholtz, W. G., Hilmas, G. E. and Zhang, S. C., Pressureless sintering of carbon-coated zirconium diboride powders. *Mater. Sci. Eng. A*, 2007, **A459**, 167–171.
71. Chamberlain, A. L., Fahrenholtz, W. G. and Hilmas, G. E., Pressureless sintering of zirconium diboride. *J. Am. Ceram. Soc.*, 2006, **89**(2), 450–456.
72. Wiley, D. E., Manning, W. R. and Hunter Jr., O., Elastic properties of polycrystalline TiB_2, ZrB_2 and HfB_2 from room temperature to 1300 K. *J. Less-Common Met.*, 1969, **18**, 149–157.
73. Cutler, R. A., Engineering properties of borides. In *Ceramics and Glasses, Engineering Materials Handbook*, *vol. 4*, ed. S. J. Schneider Jr. ASM International, Materials Park, OH, 1991, pp. 787–803.
74. Pampuch, R., *Ceramic Materials: An Introduction to Their Properties*. Elsevier Scientific Publishers/PWN-Polish Scientific Publishers, New York/Warsaw, Poland, 1976, pp. 172–190.
75. Guo, S. Q., Hirosaki, N., Yamamoto, Y., Nishimura, T. and Mitomo, M., Hot-press sintering silicon nitride with Lu_2O_3 addition: elastic moduli and fracture toughness. *J. Eur. Ceram. Soc.*, 2003, **23**, 537–545.
76. Jun, C. K. and Shaffer, P. T. B., Elastic modulus of dense silicon carbide. *Mater. Res. Bull.*, 1972, **7**(1), 63–70.
77. Nakamura, M., Matsumoto, S. and Hirano, T., Elastic constants of $MoSi_2$ and WSi_2 single crystals. *J. Mater. Sci.*, 1990, **25**, 3309–3313.
78. Rice, R. W., Particle effects on elastic properties, crack propagation, and fracture toughness of ceramic composites at ~22 °C. *Mechanical Properties of Ceramics and Composites*. Marcel Dekker, Inc., New York, 2000, 457 pp.
79. Dean, E. A. and Lopez, J. A., Empirical dependence of elastic moduli on porosity for ceramic materials. *J. Am. Ceram. Soc.*, 1983, **66**, 366–370.
80. Bert, C. W., Prediction of elastic moduli of solid with oriented porosity. *J. Mater. Sci.*, 1985, **20**, 2220–2224.
81. Jeong, H. and Hsu, D. K., Quantitative estimation of material properties of porous ceramics by means of composite micromechanics and ultrasonic velocity. *NDT Int.*, 1996, **29**(2), 95–101.
82. Guo, S. Q., Hirosaki, N., Yamamoto, Y., Nishimura, T. and Mitomo, M., Improvement of high-temperature strength of hot-pressed sintering silicon nitride with Lu_2O_3 addition. *Scripta Mater.*, 2001, **45**, 867–874.
83. Guo, S. Q., Hirosaki, N., Yamamoto, Y., Nishimura, T. and Mitomo, M., Strength retention in silicon nitride ceramics with Lu_2O_3 additives after oxidation exposure in air at 1500 °C. *J. Am. Ceram. Soc.*, 2002, **85**, 1607–1609.
84. Zimmenmann, J. W., Hilmas, G. E., Fahrenholtz, W. G., Dinwiddie, R. B., Porter, W. D. and Wang, H., Thermophysical properties of ZrB_2 and ZrB_2–SiC ceramics. *J. Am. Ceram. Soc.*, 2008, **91**(5), 1405–1411.
85. Tye, R. P. and Clougherty, E. V., The thermal and electrical conductivities of some electrically conducting compounds. In *Proceeding of the Fifth Symposium on Thermophysical Properties*, 1970, pp. 396–401.
86. Kinoshita, H., Otani, S., Kamiyama, S., Amano, H., Akasaki, I., Suda, J. and Matsunami, H., Zirconium diboride (0001) as an electrically conductive lattice matched substrate for gallium nitride. *Jpn. J. Appl. Phys.*, 2001, **40**(12A), L1280–1282.
87. Guo, S. Q., Nishimura, T., Tanaka, H. and Kagawa, Y., Thermal and electrical properties in hot-pressed ZrB_2–$MoSi_2$–SiC composites. *J. Am. Ceram. Soc.*, 2007, **90**(7), 2255–2258.
88. Loehman, R., Corral, E., Dumm, H. P., Kotula, P. and Tandon R., Ultra high temperature ceramics for hypersonic vehicle applications. SANDIA Report, SAND 2006-2925, Sandia National Laboratories, Albuquerque, New Mexico 87185 and Livermore, CA 94550, 2006.
89. Rahman, M., Wang, C. C., Chen, W., Akbar, S. A. and Mroz, C., Electrical resistivity of titanium diboride and zirconium diboride. *J. Am. Ceram. Soc.*, 1995, **78**(5), 1380–1382.
90. Samsonov, G. V. and Grebenkina, V. G., Temperature coefficient of electroresistance of some high-melting compounds. *Sov. Powder Metall. Metal Ceram.*, 1968, **7**(2), 107–111.
91. Jimbou, R., Takahashi, K., Matsushita, Y. and Kosugi, T., SiC-ZrB_2 electroconductive ceramic composite. *Adv. Ceram. Mater.*, 1986, **1**(4), 341–345.
92. Takahashi, K. and Jimbou, R., Effect of uniformity on the electrical resistivity of SiC–ZrB_2 ceramic composites. *J. Am. Ceram. Soc.*, 1987, **70**(12), C-369–C-373.
93. Jimbou, R., Suzuki, Y. and Takahashi, K., Effect of dispersion on resistivity of SiC–ZrB_2 electroconductive ceramic composites. *J. Ceram. Soc. Jpn.*, 1990, **98**(2), 225–230.